Journal of Anatomy

J. Anat. (2015) **226**, pp575–595 doi: 10.1111/joa.12303

Deconstructing cartilage shape and size into contributions from embryogenesis, metamorphosis, and tadpole and frog growth

Christopher S. Rose, Danny Murawinski and Virginia Horne

Department of Biology, James Madison University, Harrisonburg, VA, USA

Abstract

Understanding skeletal diversification involves knowing not only how skeletal rudiments are shaped embryonically, but also how skeletal shape changes throughout life. The pharyngeal arch (PA) skeleton of metamorphosing amphibians persists largely as cartilage and undergoes two phases of development (embryogenesis and metamorphosis) and two phases of growth (larval and post-metamorphic). Though embryogenesis and metamorphosis produce species-specific features of PA cartilage shape, the extents to which shape and size change during growth and metamorphosis remain unaddressed. This study uses allometric equations and thin-plate spline, relative warp and elliptic Fourier analyses to describe shape and size trajectories for the ventral PA cartilages of the frog *Xenopus laevis* in tadpole and frog growth and metamorphosis. Cartilage sizes scale negatively with body size in both growth phases and cartilage shapes scale isometrically or close to it. This implies that most species-specific aspects of cartilage shape arise in embryogenesis and metamorphosis. Contributions from growth are limited to minor changes in lower jaw (LJ) curvature that produce relative gape narrowing and widening in tadpoles and frogs, respectively, and most cartilages becoming relatively thinner. Metamorphosis involves previously unreported decreases in cartilage size as well as changes in cartilage shape. The LJ becomes slightly longer, narrower and more curved, and the adult ceratohyal emerges from deep within the resorbing tadpole ceratohyal. This contrast in shape and size changes suggests a fundamental difference in the underlying cellular pathways. The observation that variation in PA cartilage shape decreases with tadpole growth supports the hypothesis that isometric growth is required for the metamorphic remodeling of PA cartilages. It also supports the existence of shape-regulating mechanisms that are specific to PA cartilages and that resist local adaptation and phenotypic plasticity.

Key words: allometry; amphibian; cartilage; frog; growth; metamorphosis; shape change.

Introduction

The shape of skeleton is arguably the most important morphological trait for studying the evolutionary history of vertebrate animals. Although vertebrate skeletons adhere to a relatively conserved body plan (Goodrich, 1930) and have relatively few histological types (Hall, 2005), vertebrate cartilages and bones exhibit an almost boundless array of shapes (Gregory, 1933; de Beer, 1937; Carroll, 1987; Alexander, 1994; Kardong, 2012). This is because the shape of a skeletal element to a large degree reflects its function (Cuvier, after Russell, 1916; Alexander, 1994), and skeletal function is labile in both development and evolution (Murray, 1936; Carroll, 1987; Kardong, 2012). The diverse shapes of load-bearing bones and cartilages reflect the many ways that vertebrate animals feed, breath and move (Schwenk, 2000; Biewener, 2005). Skeletal elements are also shaped for many more specific functions ranging from display, protection and heat diffusion to sound production, sensory perception and reproductive behavior. In addition, skeletal shape is a major determinant of body form and of the general arrangement of musculature, nerves and blood vessels (Goodrich, 1930; de Beer, 1937; Presley, 1993; Olsson et al. 2001; Ericsson et al. 2004). The embryonic tissues that form skeleton also directly influence the development of other tissues, including muscles, nerves and epithelia (Schneider & Helms, 2003; Ericsson & Olsson, 2004; Ericsson et al. 2009). These qualities and its preservability in the fossil record make the skeleton a very large and informative dataset for describing diversification.

Correspondence
Christopher S. Rose, Department of Biology, James Madison University, Harrisonburg, VA 22807, USA. E: rosecs@jmu.edu

Accepted for publication *26 February 2015*
Article published online *25 April 2015*

Understanding this diversification requires understanding how skeletal shape develops and evolves at the level of individual tissues.

Research on the evolutionary developmental biology of skeletal shape proceeds largely on two fronts. On one front, developmental geneticists are unraveling how embryonic cells condense and differentiate into skeletal rudiments with species-specific shapes. Research on the jaw and throat, or pharyngeal arch (PA), skeleton has revealed an interplay between homeotic gene expression in migrating neural crest cells and signaling from PA tissues that determines the shape and arrangement of neural crest-derived cartilages (Gendron-Maguire & Gridley, 1993; Rijli et al. 1993; Grammatopoulos et al. 2000; Pasqualetti et al. 2000; Beverdam et al. 2002; Depew et al. 2002; Miller et al. 2003; Ruhin et al. 2003; Abzhanov & Tabin, 2004; summary by Rose, 2009). Interspecific differences in bird beak shape result from differential amounts of bone morphogenetic protein and calmodulin signaling that affect the pattern and rate of cell division within the beak condensation (Abzhanov et al. 2004, 2006; Wu et al. 2004, 2006; Mallarino et al. 2011). More recent research addresses the mechanisms underlying ontogenetic changes and interspecific and ecophenotypic differences in the shapes of limb cartilages and bones (Farnum et al. 2008a,b; Cooper et al. 2013; Serrat, 2014).

On the other front, functional and developmental morphologists have long used exponential equations to describe patterns of bone growth and variation in bone shape (Galilei, 1638; Huxley, 1932; Gould, 1966; McNamara, 1982; Schmidt-Nielsen, 1984; Strauss, 1993). Growth allometries that relate bone shape to body size at different stages within a species show that mammal limb bones generally become relatively thinner as they grow (Biewener, 2005). In contrast, static allometries that relate bone shape to body size in the adults of related species show that small and large species of mammals and birds generally have bones of similar shape (McMahon, 1973, 1975; Alexander et al. 1979; Prange et al. 1979; Prothero & Sereno, 1982; Prothero, 1992; Biewener, 2005). Allometries are also used to look for differences that arise independently of body size between the sexes, between experimental and control animals, and among related taxa (Gould, 1974; McFadden et al. 1986; Kieser & Groeneveld, 1992; Pyenson et al. 2013).

Understanding the relative contributions of development and growth to skeletal shape requires bringing these two research approaches together, a task for which the PA skeleton of amphibians is particularly well suited. PA skeletons are formed entirely from cranial neural crest cells that migrate into pharyngeal arches (Sadaghiani & Thiébaud, 1987; Hall, 1999). Their embryonic formation is largely complete by the pharyngula stage, when vertebrate embryos have generally conserved morphologies (von Baer, 1828; Haeckel, 1880; Ballard, 1981) and gene expression (Irie & Kuratani, 2011), yet the shapes of adult PA skeletons vary dramatically among taxa (de Beer, 1937). Also, amphibian PA skeletons consist largely of rod-, bar- and plate-shaped elements that, unlike other parts of the skull, do not lie adjacent to sense organs or brain and persist mostly as cartilage until after metamorphosis (Rose, 2009). These conditions help narrow the focus to how cartilage cells alone contribute to cartilage growth and shape change. Cartilage differs from bone in being sealed off, i.e. not penetrated by nerves or blood vessels, and growing via cell behaviors inside the tissue as well as on its surface (Hall, 2005; Rose, 2009). Cartilage shape is thus an emergent property arising from the collective activities of all cells that contribute to the cartilage throughout life (Rose, 2009).

The amphibian PA skeleton is also uniquely required to support feeding and breathing in two habitats, an aquatic one followed by a terrestrial one. It thus undergoes two periods of development: embryogenesis and metamorphosis; and two periods of growth: larval and post-metamorphic. Whereas embryogenesis typically involves the patterning and differentiation of new skeletal elements, metamorphosis additionally involves loss and change in the size, shape and arrangement of existing elements (Rose & Reiss, 1993; Rose, 2003). Having multiple periods of development and growth suggests more opportunity for phylogenetic diversification. Indeed, amphibian PA elements show pronounced interspecific differences in PA skeletal shape that arise during metamorphosis as well as embryogenesis (Smith, 1920; Wilder, 1925; Wassersug & Hoff, 1982; Ruibal & Thomas, 1988; Haas et al. 2006, 2014; Ziermann et al. 2013). Further, the embryonic repatterning of certain larval elements and the metamorphic appearance of a new adult element have been identified as key innovations in salamander evolution (Wake, 1982; Alberch & Gale, 1986; Alberch, 1987).

Despite many anatomical descriptions of PA skeletal development in metamorphosing frogs and salamanders (Pusey, 1938; Sedra & Michael, 1957, 1958; van der Westhuizen, 1961; Chacko, 1965a; Wassersug & Hoff, 1982; Wiens, 1989; Hall & Larsen, 1998; Haas, 1999; Rose, 2003), there has been little attempt to quantify changes in the shape and size of individual elements or to assess the contribution of growth to species-specific features of skeletal shape. This study uses allometric equations and thin-plate spline (TPSA), relative warp (RWA) and elliptic Fourier (EFA) analyses to describe shape and size changes of the ventral PA cartilages of the frog *Xenopus laevis* in tadpole and frog growth and metamorphosis. These cartilages in tadpoles include in the lower jaw (LJ) Meckels cartilage (MC) and the infrarostral cartilage (IR), the ceratohyal (CH) and the branchial arch cartilages (BA). These cartilages have distinct larval shapes and remodel differently at metamorphosis: the LJ and CH acquire new adult shapes, and the BA are replaced by alar and thyroid processes (AP, TP; Sedra & Michael, 1957). This study also compares shape changes in larval and post-metamorphic growth, examines the effects of growth and development on shape variation in larvae, and distinguishes

between changes in cartilage size and shape at metamorphosis.

Materials and methods

Specimen rearing

Specimens were produced from overnight matings of *Xenopus laevis* injected with 200–500 units of human chorionic gonadotropin (Sigma, St Louis, MI, USA; C1063); females were preinjected with 50–100 units of pregnant mares serum gonadotropin (Sigma G4877) 4 days previously. Tadpoles and metamorphosing specimens were reared under natural lighting at room temperature (22–24 °C) in 0.1 × Marc's Modified Ringers, and fed every 1–2 days with a blended suspension of Frog Brittle for Tadpoles (NASCO); partial water changes were done every week. Frogs were raised at 18–20 °C under a 12 : 12 h light : dark cycle in dechlorinated tap water, and fed Sinking Frog Pellets (Xenopus Express); complete water changes were done every 2–3 days. Tadpoles and most frogs were sampled at regular intervals, killed by a 5-min immersion in 0.2% MS222 (Sigma), fixed for 24 h in 10% neutral buffered formalin, and staged using the Nieuwkoop Faber (NF) staging system for *Xenopus laevis* (Nieuwkoop & Faber, 1956). Some frogs died from natural causes in the lab colony, and some males were killed in 0.2% benzocaine (Sigma) and frozen prior to fixation.

The specimens used to quantify cartilage size and shape changes throughout life included 4–10 individuals for each stage from NF 46 to 66 (145 in total) and 28 frogs ranging from 2 weeks after NF 66 to adult. The frogs included 13 males with snout–vent lengths (SVLs) of 18–66 mm and 12 females with SVLs of 20–118 mm. The specimens used to control for differences in body size when estimating changes in cartilage size and shape at metamorphosis included 36 at NF 58/59 and 32 at NF 66; the latter were anesthetized in 0.1% benzocaine for photographing at NF 58/59. This research has received IACUC approval and conforms to NIH guidelines.

Data collection

To obtain body size in tadpoles and metamorphs, measurements were taken from ventral-view photographs of anesthetized or killed specimens using the criteria in Appendix 1 and Fig. 1a. Snout–belly length (SBL) was selected over SVL as the vent is difficult to identify in ventral-view in small tadpoles and SVL is inflated by disproportionate growth of the hind legs in large tadpoles. To obtain head size in the NF 58/9 specimens used to control for differences in body size, two measures of head width and one of head length were obtained from photographs (Appendix 2; Fig. 1a) and summed. To obtain body size in frogs, SVLs were measured using calipers. When possible, frogs were sexed using the presence of cloacal lips and differentiated gonads.

To obtain skeletal data, heads or entire specimens were stained with Alcian blue for cartilage and Alizarin red for bone, and cleared in glycerol. PA skeletons were photographed in ventral view before and after dissection; the pre-dissection photographs were taken as a precaution against possible damage to PA elements during dissection and to test for shape distortion due to dissection. All photos were taken using a Zeiss Stemi SV 11 dissecting scope. Landmarks for the MC, IR, CH, BA, AP and TP were marked on post-dissection photographs using Adobe Photoshop following the criteria in Appendix 1 and Fig. 1b–e. Landmarks were then digitized using NIH ImageJ, and the *X*- and *Y*-coordinates were used to calculate cartilage dimensions in Microsoft Excel. The dimensions for paired structures were averaged before analysis. Replicate data for estimating measurement error were collected from three replicate photographs for each of a NF 46, 54 and 59 specimen; the cartilages were repositioned in the glycerol prior to each photograph. Replicates were included in all analyses.

Bivariate analyses

Allometric equations of the form $y = mx^{\alpha}$ were calculated for tadpoles and frogs by ordinary least-squares regression of log-transformed dimensions. The pairs of dependent and independent variables selected for this analysis included the greatest dimensions of skeletal elements and body size, the minor and major dimensions of the rectangles that enclose each element, and specific widths of elements and their greatest dimension (see Fig. 1 and Appendices 1 and 2 for specific dimensions). Allometries were compared using SAS 9.3 to test for significant differences in α, which is the slope of a linear regression equation generated using log-transformed dimensions. A general linear model with group and interaction terms was used to test for differences between stages, between sexes and among cartilages within a stage. A general linear model with a MTEST statement was used to test for differences among multiple dependent variables regressed against the same independent variable, for example multiple widths of a cartilage regressed against its maximum dimension. The 95% confidence limits for α were also calculated to identify values that differed from 1 at $P = 0.05$.

Multivariate analyses

Multivariate analyses were done on larval elements using right and reflected left elements, meaning that each specimen was represented by two right-sided shapes (which appear left-sided in the conventional ventral view of PA elements).

Thin-plate spline analyses and RWAs were performed for the larval LJ, CH and BA ($N = 174, 172, 144$) using the shapes package for R (Dryden, 2013) and tpsRelw (Rohlf, 2013); landmark coordinates were first corrected for differences in shape size, position and orientation by generalized Procrustes analysis in R. TPSA compares two configurations of landmarks by interpolating differences in the spacing of homologous landmarks to produce a deformation grid that reveals global (or uniform) and local (or non-uniform) differences between the two configurations. It further deconstructs the non-uniform deformation into separate components at different spatial scales (partial warps) and calculates their relative contributions to the total deformation (partial warp scores; Zelditch et al. 2004). RWA is a principal component analysis of the partial warps scores that are generated by deforming the average configuration for a sample of shapes to fit the landmark configurations of each individual shape.

Elliptic Fourier analyses were performed for the larval CH and BA ($N = 154, 132$) using SHAPE 1.3 (Iwata & Ukai, 2002). EFA calculates the coefficients of sine and cosine waves that when added together reconstruct the two curves that are created for a shape by plotting its *X*- and *Y*-values as functions of distance traveled along the shape or contour (Kuhl & Giardina, 1982). Typically, each *X*-curve and each *Y*-curve are reconstructed from 10 sine and 10 cosine waves with wavelengths of 1, 1/2, 1/3, ..., 1/10 × the total distance along the contour. The first three coefficients generated for each contour are always 1 or 0, so only the remaining 37 coefficients are used for principal component analysis.

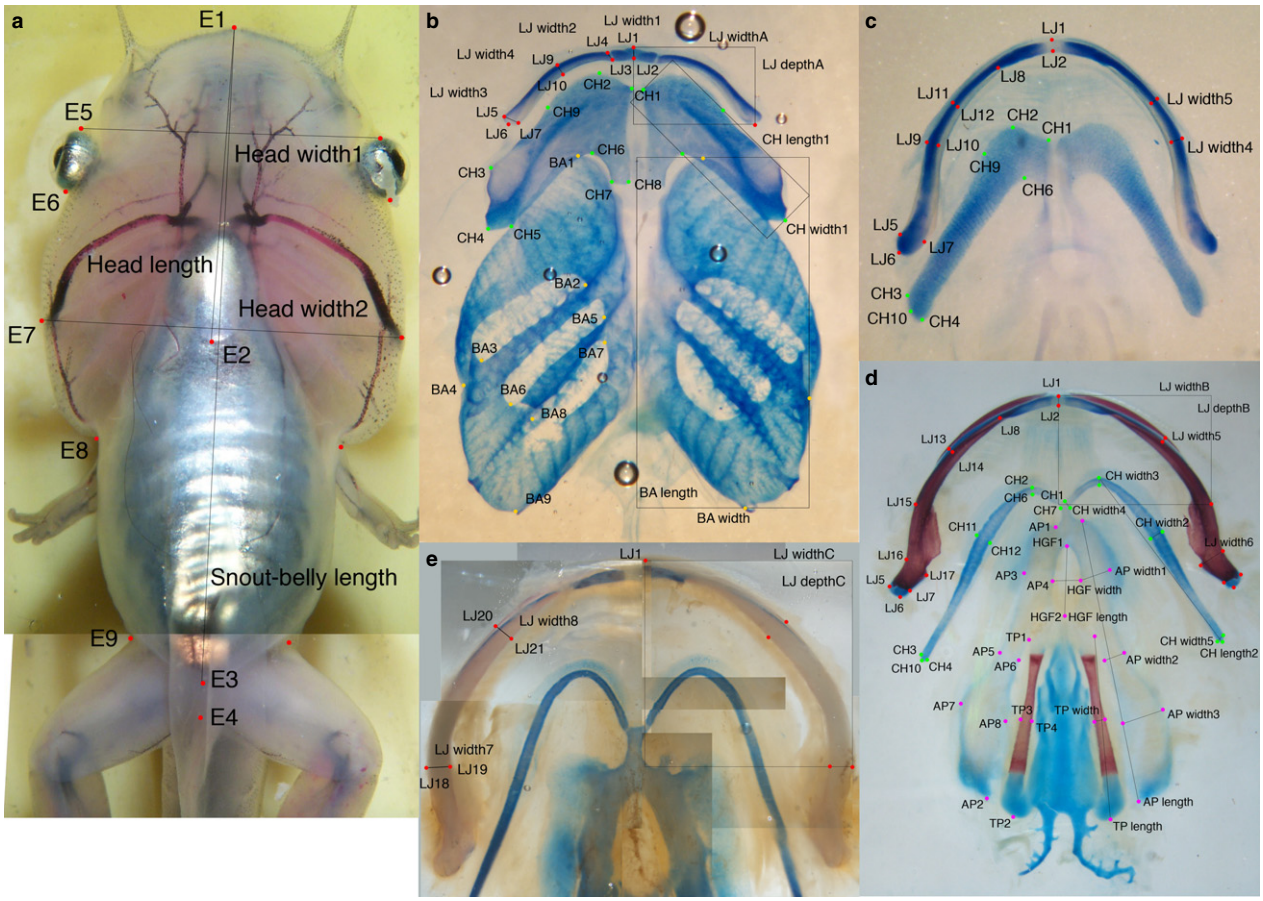

Fig. 1 Landmarks and dimensions used for morphometric analyses. Landmarks and dimensions used to measure body size and head size in NF stages ≤ 66 (a) and size and shape of lower jaw skeleton (LJ), ceratohyal (CH), branchial arch (BA), alar process (AP) and thyroid process (TP) cartilages and hyoglossal foramen (HGF) in NF stages 46–59 (b), 59–66 (c), 66+ to adults (d) and medium to large adults (e). All landmark and dimensions are described in Appendices 1 and 2.

To identify the extreme shapes in each principal component analysis, Mahalanobis distances were calculated in SAS 9.3 using the first five principal component scores. This measure shows how far each individual shape is from the average shape after correcting the principal component scores for unequal variance along and unequal covariance among the different component axes.

Results

Anatomy and general observations

Though well described in the literature (Sedra & Michael, 1957; Trueb & Hanken, 1992), the anatomy of the ventral PA skeleton of *Xenopus* is reviewed here to provide background for shape and size changes that have not been described previously. In tadpoles (Fig. 2), the LJ is comprised of a small median infrarostral and long, gently curving MC that together resemble half of an archer's bow in frontal view; each has a blocky outline in sections perpendicular to its central axis. The CH is a broad bar with uniquely irregular outlines at each point along its central axis. The four BA, which are treated here as one unit, are fused medially and laterally, and each has a dorsal process with finely branching surfaces (gill filters) that support food collecting and respiratory epithelia (Gradwell, 1975). The dorsal processes of the anterior- and posterior-most BA have smooth outer surfaces that are continuous with dorsal expansions of the fused medial and lateral edges, forming an enclosed space or branchial basket.

In frogs (Fig. 2), the MC and infrarostral are indistinguishably fused, and the LJ resembles half of a U in frontal view, has a cylindrical outline and is fully encased by dermal bones. The CH is a slender, almost straight rod referred to as the hyale (though the term CH is used here to facilitate tadpole–frog comparisons). The BAs have been replaced medially by a hyoglossal plate with a hyoglossal foramen (HGF) and laterally by two paired posterolaterally aligned processes, the AP and TP. The AP is plate-like and wider posteriorly than anteriorly, and the TP is cylindrical and resembles a long bone in becoming endochondrally ossified in its middle region. The larynx and the plate-like 'lamellae of juvenile cartilage' that appear along anterior edges of the CH and AP in older frogs (Fig. 1e; see also Sedra & Michael,

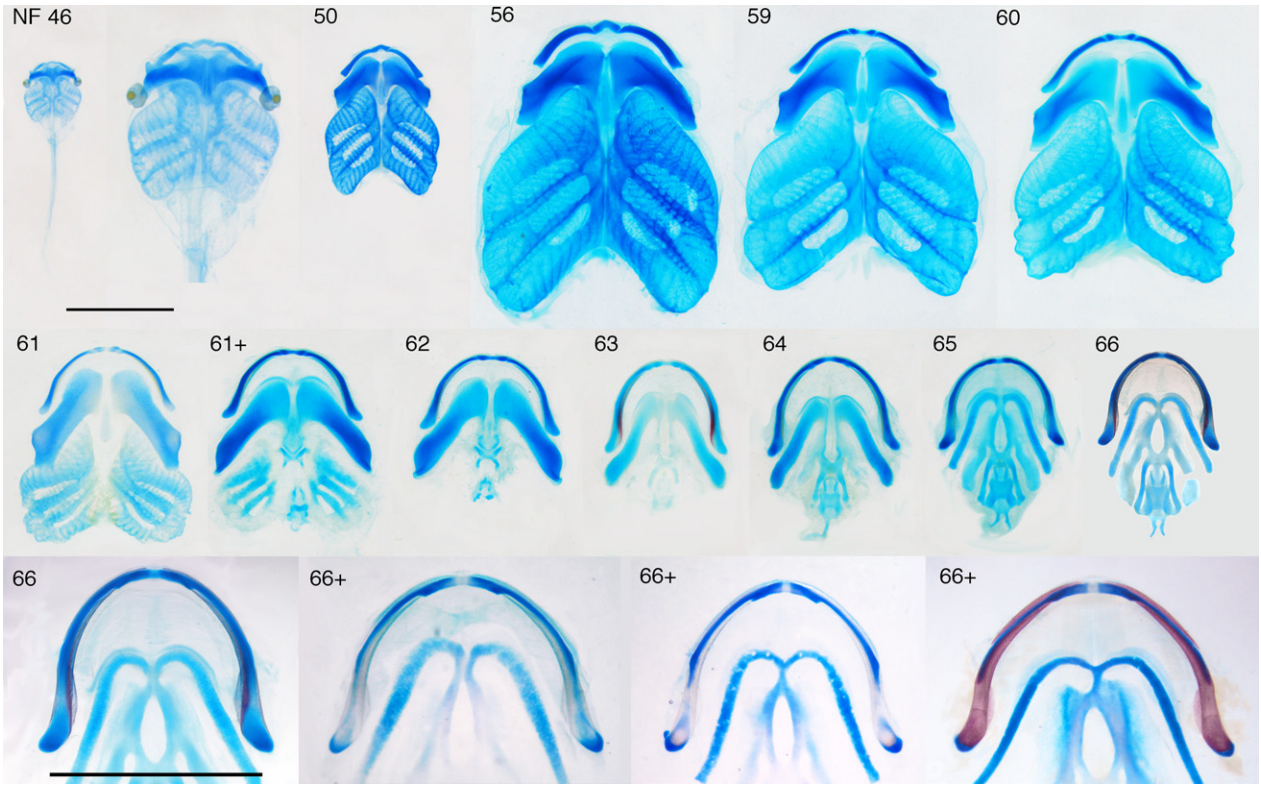

Fig. 2 Series of dissected, skeletally stained PA skeletons from NF stages 46 to 66+. Ventral views, blue is cartilage, red is bone, scale bars are 5 mm and apply to all panels, except the second one in which the NF 46 skeleton is expanded to be comparable in size with the NF 50 skeleton, the NF 46 skeleton was not dissected because of its small size. NF 46–59 covers tadpole growth, NF 59–66 covers metamorphosis and the NF 66–66+ series shows the separation of the LJ cartilage into two pieces at the end of metamorphosis.

1957) are not included in this study because of difficulty in distinguishing their parts or edges and inconsistent chondrification.

The rate of change in cartilage shape changes abruptly at NF 59 for all three larval elements, and at NF 66 for the LJ and CH (Fig. 3a); the change at NF 66 is difficult to show graphically as body size decreases from NF 59 to 66 and increases thereafter and no stages are available after NF 66. NF 59 and 66 were thus used to demarcate three stage categories for analyzing cartilage size and shape change: tadpole growth (NF 46–59); metamorphosis (NF 59–66); and frog growth (≥ NF 66). This contrasts with the staging table for *Xenopus laevis*, which recognizes metamorphosis as starting at NF 58 (Nieuwkoop & Faber, 1956). As NF 59 and NF 66 specimens were each included in two categories, they were assigned both kinds of landmarks.

Most regressions of log-transformed dimensions yielded *R*-values above 0.90 (Tables 1–5), indicating that relationships generally fit the model $y = mx^{\alpha}$. Replicate measurements of dimensions indicated precision ranges of ± 2–7 and 10–50 μm for the cartilage dimensions of NF 46 and 59 tadpoles, respectively; these values correspond to ± 0.2–1.0% of the largest cartilage dimensions. TPS deformation grids comparing cartilages before and after dissection (not shown) indicated negligible effects of dissection on shape for all elements.

Cartilage size and shape in tadpole growth (NF 46–59)

The greatest dimensions of the tadpole LJ, CH and BA all scale negatively with body size (Fig. 3c) and with significantly different α-values from each other (Table 1).

The general shapes of the LJ, CH and BA as defined by their enclosing rectangles (Fig. 1b) scale at or close to isometry (Fig. 3d; Table 2). Whereas the CH rectangle scales with isometry (meaning that the α-value for relating CH width to length is not significantly different from 1), the LJ rectangle increases relatively faster in depth than width and the BA rectangle increases relatively slower in width than length. The four width measurements of the LJ scale negatively with LJ size, meaning that both the MC and infrarostral become relatively thinner with growth (Fig. 3e; Table 3). According to the α-values, relative thinning of the MC is greatest in the central part (width4) and least near the joint (width3).

Thin-plate spline analysis grids that deform average NF 46 shapes to fit average NF 59 shapes and comparisons of

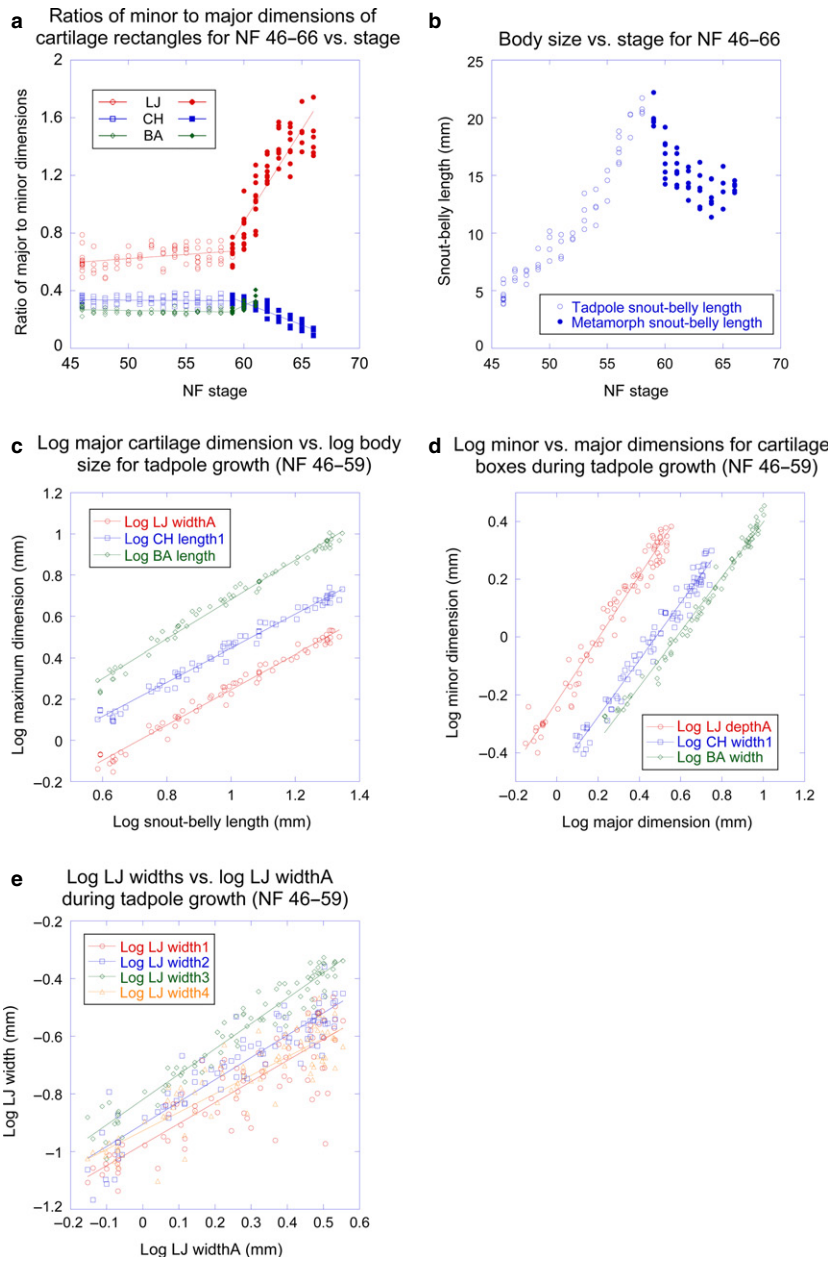

Fig. 3 Size and shape trajectories for body size and PA skeleton for tadpoles and metamorphs. (a) Ratios of minor to major dimensions of lower jaw (LJ), ceratohyal (CH) and branchial arch (BA) cartilage rectangles vs. stage for tadpoles and metamorphs; (b) body size vs. stage for tadpoles and metamorphs; (c) log of major dimension of LJ, CH and BA vs. log of body size for tadpoles; (d) log of minor dimension of LJ, CH and BA cartilage rectangles vs. log of their major dimension for tadpoles; (e) log of LJ widths vs. log of LJ greatest dimension for tadpoles.

EFA-generated average contours for these stages (Fig. 4) both support the shape changes indicated by the allometric analysis. The grids, which average left- and right-side shapes (Fig. 4a–c), additionally reveal minor changes in relative size and orientation of parts within each element. The infrarostral becomes relatively smaller and more laterally aligned, and the posteromedial process of the CH and posterior tip of the B shift laterally. Comparing average contours (Fig. 4d,e) additionally reveals features that are slight or non-evident at NF 46 becoming more pronounced at NF 59. These include concavities on the medial and lateral edges of the CH and the lateral indentation of the BA, which accommodates the systemic aortic arch artery (E7 in Fig. 1a). TPS grids produced using separate left and right elements reveal slight changes in orientation of the CH and BA relative to the body (Fig. 4f-h). The CH becomes aligned more longitudinally and the BA becomes aligned more laterally. Grids comparing average shapes for consecutive stages from NF 46 to 59 (not shown) indicate that shape changes gradually in growth and there is no noticeable change associated with the appearance at NF 55 of the medial angulosplenial bone next to the MC and its subsequent growth.

The first and second principle components of RWAs for the LJ, CH and BA (Fig. 5a,e,m) and of EFAs for the CH and BA (Fig. 5i,q) explain 36–56% and 16–26% of the variation in shapes, respectively. Comparing the lowest and highest stages in each analysis (Fig. 5b,f,j,n,r), NF 46 shapes have little or no overlap with NF 59 shapes and have a larger

Table 1 Regression data for major cartilage dimensions vs. body size in tadpoles and frogs.

Tadpoles	α	*R*	*N*	Frogs	α	*R*	*N*	*P*-value for tadpoles and frogs having the same α
LJ widthA vs. sbl	0.857	0.991	73	Bony LJ widthA vs. svl	0.861	0.989	32	0.8750 (*N* = 105)
CH length1 vs. sbl	0.825	0.992	73	CH length2 vs. svl	0.896	0.985	30	0.0106 (*N* = 103)
BA length vs. sbl	0.954	0.993	68	AP length vs. svl	1.006*	0.994	29	
				TP length vs. svl	1.143	0.973	29	
P-value for regressions above having the same α		< 0.0001 (*N* = 67)		*P*-value for four regressions above having the same α		< 0.0001 (*N* = 25)		
				Cart. LJ widthB vs. svl	0.820	0.992	31	
				Bony LJ depthA vs. svl	0.903	0.991	32	
				HGF length vs. svl	0.848	0.976	29	

AP, alar process; BA, branchial arch cartilage; CH, ceratohyal cartilage; HGF, hyoglossal foramen; LJ, lower jaw; TP, thyroid process.
*α not significantly different from 1 at *P* = 0.05.

Table 2 Regression data for major vs. minor dimensions of element-enclosing rectangles in tadpoles and frogs.

Tadpoles	α	*R*	*N*	Frogs	α	*R*	*N*	*P*-value for tadpoles and frogs having the same α
LJ depthA vs. widthA	1.089	0.983	87	Bony LJ depthA vs. widthA	1.013*	0.981	33	0.0713 (*N* = 120)
CH width1 vs. length1	0.985*	0.985	87	CH width2 vs. length2	0.464	0.771	31	0.0117 (*N* = 118)
BA width vs. length	0.947	0.993	82	Cartilage LJ depthB vs. widthB	0.619	0.938	31	
P-value for regressions above having same α		0.0053 (*N* = 256)		Bony LJ depthC vs. widthC	1.023*	0.955	8	

BA, branchial arch cartilage; CH, ceratohyal cartilage; LJ, lower jaw.
*α not significantly different from 1 at *P* = 0.05.

Table 3 Regression data for other skeletal dimensions in tadpoles and frogs.

Tadpoles	α	*R*	*N*	Frogs	α	*R*	*N*
LJ width1 vs. widthA	0.729	0.856	87	Cartilage LJ width5 vs. widthB	0.424	0.596	31
LJ width2 vs. widthA	0.772	0.925	87	Bony LJ width6 vs. widthA	0.916*	0.963	33
LJ width3 vs. widthA	0.880	0.972	87	Bony LJ width7 vs. widthA	0.662	0.639	8
LJ width4 vs. widthA	0.641	0.888	87	Bony LJ width8 vs. widthA	0.664	0.836	8
P-value for four regressions above having the same α		< 0.0001 (*N* = 87)		CH width2 vs. length2	0.464	0.771	31
				CH width3 vs. length2	0.497	0.770	31
				CH width4 vs. length2	0.845	0.904	31
				CH width5 vs. length2	0.433	0.699	31
				P-value for four regressions above having the same α		< 0.0001 (*N* = 31)	
				AP width1 vs. length	0.900*	0.874	30
				AP width2 vs. length	0.950*	0.903	30
				AP width3 vs. length	1.262	0.974	30
				P-value for three regressions above having the same α		0.001 (*N* = 30)	
				TP width vs. length	0.858	0.975	30
				HGF width vs. length	0.948*	0.611	30

AP, alar process; CH, ceratohyal cartilage; HGF, hyoglossal foramen; LJ, lower jaw; TP, thyroid process.
*Not significantly different from 1 at *P* = 0.05.

Table 4 Regression data for major cartilage dimensions vs. body size in male and female frogs.

Regression	Males			Females			*P*-value for males and females having the same α
	α	*R*	*N*	α	*R*	*N*	
Bony LJ depthA vs. svl	0.951*	0.992	13	0.960*	0.995	11	0.8431 (*N* = 24)
CH length vs. svl	0.885*	0.967	12	0.936*	0.989	11	0.5667 (*N* = 23)
AP length vs. svl	0.946*	0.993	12	1.009*	0.997	12	0.1878 (*N* = 24)
TP length vs. svl	1.273	0.980	12	1.047*	0.997	12	0.0080 (*N* = 24)
HGF length vs. svl	0.934*	0.953	12	0.880	0.991	12	0.5631 (*N* = 24)

AP, alar process; CH, ceratohyal cartilage; HGF, hyoglossal foramen; LJ, lower jaw; TP, thyroid process.
*α not significantly different from 1 at $P = 0.05$.

Table 5 Regression data for cartilage widths vs. lengths in male and female frogs.

Regression	Males			Females			*P*-value for males and females having the same α
	α	*R*	*N*	α	*R*	*N*	
Bony LJ widthA vs. depthA	0.886	0.965	13	0.877	0.997	11	0.8946 (*N* = 24)
CH width2 vs. length2	0.352	0.557	12	0.578	0.931	11	0.2063 (*N* = 23)
CH width3 vs. length2	0.497	0.890	12	0.693	0.956	11	0.1016 (*N* = 23)
CH width4 vs. length2	0.976	0.917	12	0.987	0.973	11	0.9345 (*N* = 23)
CH width5 vs. length2	0.149	0.257	12	0.651	0.912	11	0.0190 (*N* = 23)
AP width1 vs. length	1.139	0.797	12	0.890	0.909	12	0.3925 (*N* = 24)
AP width2 vs. length	0.913	0.745	12	0.986	0.960	12	0.7674 (*N* = 24)
AP width3 vs. length	1.112	0.957	12	1.226	0.987	12	0.3702 (*N* = 24)
TP width vs. length	0.878	0.967	12	0.906	0.975	12	0.7903 (*N* = 24)
HGF width vs. length	0.671	0.490	12	1.052	0.667	12	0.5036 (*N* = 24)

AP, alar process; CH, ceratohyal cartilage; HGF, hyoglossal foramen; LJ, lower jaw; TP, thyroid process.

spread for all elements in all analyses except the CH in EFA and the BA in RWA. The spreads of replicates for NF 46 and NF 59 shapes fall well within the overall spreads for each stage. Comparing the three stages with the greatest ranges in relative size among specimens (and thus signifying the greatest potential for prolonged growth within a stage), the shapes generally separate by size, with the largest shapes usually falling closest to the center of the spread for all stages (Fig. 5c,g,k,o,s). The separation of shapes by size is most apparent for NF 46 shapes of the BA (Fig. 5o,s).

The most extreme shapes in each multivariate analysis as identified by Mahalanobis distances are disproportionately represented by NF 46–48 stages. Of the 10% of most extreme shapes, one-third belong to NF 46–48 in the EFA of the CH and two-thirds belong to these stages in the other four analyses (data not shown). This compares with none of the 17–27% of least extreme shapes belonging to NF 46–48 in four analyses and one-sixth of the 10% of least extreme shapes belonging to these stages in the RWA of the CH. Also, the NF 46–48 shapes generally cover half or more of the spreads of all stages (compare Fig. 5d,h,l,p,t with Fig. 5a,e,i,m,q), indicating that NF 46–48 shapes are relatively diverse. Correlations between Mahalanobis distances produced for the same shapes by RWA and EFA are weak ($R = 0.60$ for CH, 0.58 for BA), indicating that although the two techniques reveal similar trends with respect to stage, they vary in their resolution of individual differences.

Cartilage size and shape in metamorphosis (NF 59–66)

Cartilage size and shape changes could not be quantified for metamorphosis in the same way as for tadpole growth for several reasons. Landmarks disappear or become otherwise unrecognizable (compare Fig. 1b,c; Appendix 1) as a result of changes in surface topography from growth and resorption within cartilages as well as on their surfaces (Rose, 2009). Stage, which is the most appropriate variable for representing developmental progress, is ordinal and thus inappropriate for descriptive or inferential statistics. Finding a size measurement to gauge developmental progress is confounded by profound changes in head and body shape. Also, studies of internal anatomy require cross-sectional data, which introduce variability in body size. Unlike the starting body size for tadpole growth, which is relatively uniform among individuals, the starting body size for metamorphosis can vary considerably as a result of variation in tadpole growth and developmental rates (Fig. 3b; Wilbur

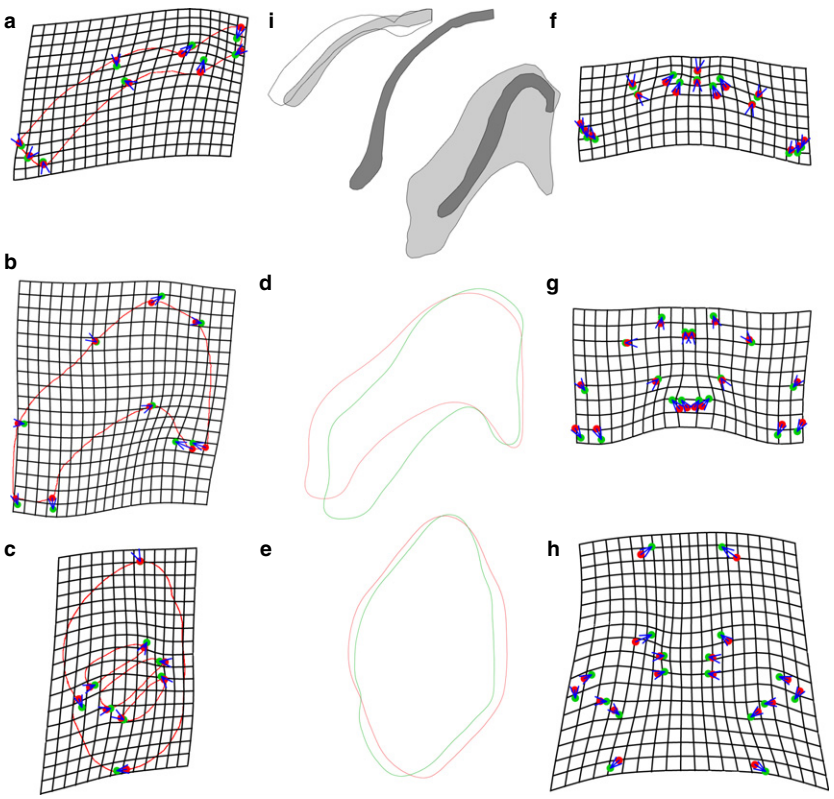

Fig. 4 TPSA deformation grids, average contours and representative outlines for the lower jaw (LJ), ceratohyal (CH) and branchial arch (BA) cartilages in tadpoles and metamorphs. (a–c) Grids showing deformation of landmarks from NF 46 (red) to 59 (green) average configurations for LJ (a), CH (b) and BA (c). (d,e) elliptic Fourier-generated average shapes for CH (d) and BA (e) at NF 46 (red) and 59 (green). (f-h), same as (a-c) but with left and right shapes analyzed separately to show changes in orientation of cartilages. (i) outlines of representative LJ and CH shapes at NF 46 (no stipple), 59 (light stipple) and 66 (dark stipple). The NF 46 LJ is drawn with the same anterior-posterior dimension as the NF 59 LJ; the NF 59 and 66 LJ and CH are from a pair of specimens with the same size at NF 59.

& Collins, 1973; Rose, 2005, 2014). Additionally, as researchers might not appreciate the degree to which body size decreases in frog metamorphosis, they could unwittingly sample larger specimens at later metamorphic stages in an effort to obtain a series of similarly sized specimens.

The following strategy was devised to control for body size variation in cross-sectional data. Of 68 specimens that were anesthetized and photographed at NF 58/59, 36 were immediately processed for morphometric analysis and 32 were reared to NF 66 and then processed for morphometric analysis. Of the 1152 possible pairings of NF 58/59 and 66 specimens, the 12 pairs whose members differed in head size at NF 58/59 by $< 1.7\%$ were selected to estimate the changes in LJ and CH dimensions that occur within individuals between NF 58/59 and NF 66. Figure 4i shows the shape and relative size of the LJ cartilages and CH for members of one pair.

Based on these pairs, the rectangle enclosing the LJ becomes on average 83% deeper and 11% narrower (ranges are 56–109% and 6–15%). Although the LJ appears to become significantly longer, its inner and outer edges increase by only 35% and 26%, respectively (28–41% and 17–33%). The LJ also becomes more tightly curved than in tadpoles, especially in the portion medial to a new inflection point at landmarks LJ9 and LJ10 (Figs 1c and 2). The middle portion of the MC (width4) becomes 27% thinner (23–37%) and the volume of the MC + IR is estimated to become 22% smaller (6–40%); this calculation is based on the MC and IR having rectangular cross-sections at NF 58/9 and circular cross-sections at NF 66 (data not shown). The infrarostral fuses to MC and the posteromedial surface of the fused cartilage acquires a ridge that abuts laterally with the tip of the angulosplenial bone as described elsewhere (Fig. 2; Sedra & Michael, 1957; Trueb & Hanken, 1992). Also, the distal tip of the LJ separates from the rest of the cartilage soon after NF 66 (Fig. 2). This separation appears to involve cartilage resorption and inward growth of the angulosplenial bone, rather than endochondral replacement.

Based on the NF 58/59–66 pairs, the CH becomes 20% shorter and 74% thinner (6–26% and 58–86%), producing a frog CH that was fully contained within the boundaries of the tadpole CH, cylindrical and more longitudinally aligned than the tadpole CH (Figs 2 and 4i). The BAs are resorbed and replaced by newly chondrifying APs, TPs and a hyoglossal plate with a central foramen (HGF).

Skeleton size and shape in frog growth (≥ NF 66)

The mandible (bony LJ) is comprised primarily of dentary bone in its anterolateral part and angulosplenial bone in its anteromedial and posterior parts (Fig. 2; Trueb & Hanken, 1992). Subdivision of the cartilage in the LJ after NF 66 produces two pieces that persist to adulthood as a posterolateral bulb of cartilage in the distal tip of the mandible and a thin rod of cartilage (cartilage LJ) in its anterior portion.

The greatest dimensions of the bony LJ, CH, AP, TP and HGF scale differently from each other with respect to body size (Fig. 6a; Table 1). Whereas greatest dimensions of the

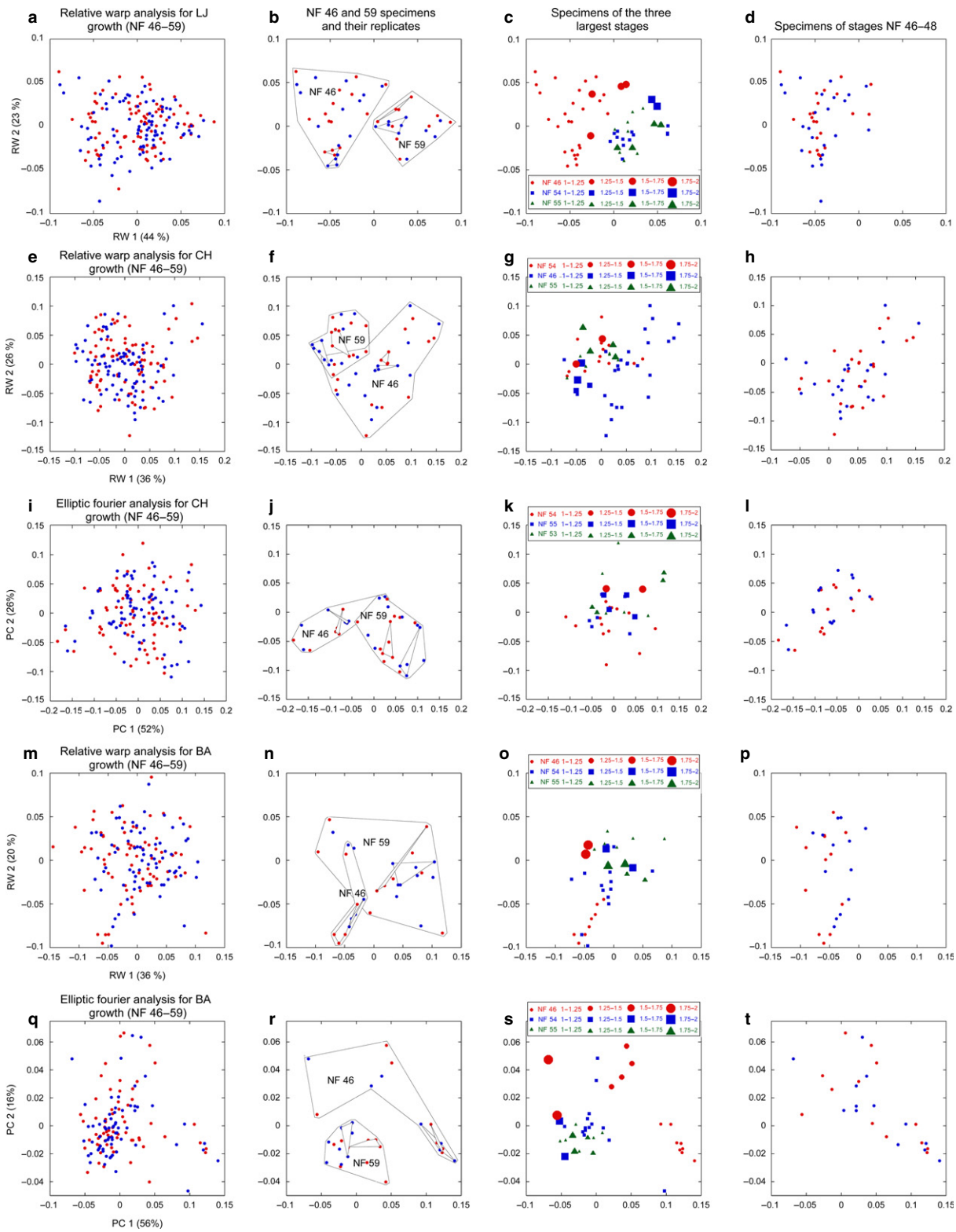

Fig. 5 Scatterplots of first and second principal component scores from RWA and EFA of the lower jaw (LJ), ceratohyal (CH) and branchial arch (BA) cartilages in tadpoles. (a–d) RWA of LJ, (e–h) RWA of CH, (i–l) EFA of CH, (m–p) RWA of BA, (q–t) EFA of BA. (a, e, i, m and q) Scores for all left (red) and right (blue) cartilages at NF 46–59 (percentages in parentheses indicate variation explained by each component). (b, f, j, n and r) Scores for only the NF 46 and 59 cartilages (larger groups) including the NF 46 and 59 replicates (smaller groups). (c, g, k, o and s) Scores for only the three stages with the largest relative size ranges (symbol sizes indicate sizes of cartilages relative to the smallest cartilage at each stage). (d, h, l, p and t) Scores for only the NF 46–48 cartilages.

bony LJ, CH and HGF scale negatively, AP length, which is the largest dimension of the entire PA skeleton, scales isometrically and TP length scales positively (Table 1). When separated by sex, all greatest dimensions scale isometrically with two exceptions: TP length scales positively in males and HGF length scales negatively in females (Table 4).

As defined by their enclosing rectangles (Fig. 6b; Table 2), the bony LJ scales isometrically and the cartilage LJ increases slower in depth than width. This means that as it grows, the cartilage LJ does not keep pace with the bony LJ and becomes increasingly confined to the anteromedial portion of the mandible (Fig. 7a). The cartilage LJ also becomes relatively thinner in the one portion where its width is measureable (width5, Table 3) and the bony LJ becomes relatively thinner outside the joint region (widths7 and 8). At SVLs of 38–44 mm, the curvature of the bony LJ increases near the joint so that the widest part of the gape moves anterior of the jaw joint (Fig. 7a). The rectangle that encloses the new most lateral and anterior points of the bony LJ also scales isometrically (Fig. 6b; Table 2), meaning that the new curvature is retained to larger sizes.

The four widths of the CH scale negatively with CH length and its relative thinning is much greater than in other cartilages except where the CH attaches to the hyoglossal plate (width4, Figs 6c and 7b; Table 3). The anterior portion of the AP and the HGF scale isometrically, the posterior portion of the AP becomes relatively wider, and the TP becomes relatively thinner (Fig. 6d; Table 3).

When the bony LJ, CH, AP, TP and HGF are separated by sex, males have lower α-values for most width-to-length regressions than females (Table 5). However, the only α-value that is significantly lower ($P = 0.01$) is for the male CH width at its distal tip (width5), and this relationship also has an exceptionally low R-value. The α-values for the male and female TP width-to-length regressions are very similar (Fig. 6e), indicating that once males attain a larger TP (which appears to happen before gonad differentiation and hence before the sexes could be distinguished in this study), male and female TPs follow the same rate of relative thinning.

Discussion

The functional significance of cartilage size scaling

Isometric or slightly negative scaling of PA skeleton size with body size is consistent with previous studies on *Xenopus* (Ryerson & Deban, 2010), not unusual for frogs (Larson, 2005) or other vertebrates (Radinsky, 1981) and not unexpected when exogenous feeding is critical at the onset of growth and trophic demands do not change substantially with growth (Emerson & Bramble, 1993). The LJ and CH of *Xenopus* tadpoles are continually pumping when food is available to maintain water flow through the buccopharyngeal cavity (Gradwell, 1971, 1975). Unlike most tadpoles, *Xenopus* lacks gill filaments and relies upon an overdeveloped and relatively immobile branchial skeleton with finely elaborated gill filters and food traps to remove particles from the flow and transfer them to the esophagus (Seale et al. 1982). The BA surfaces have a secondary role in gas exchange, which proceeds primarily through cutaneous respiration and lung breathing (Feder & Wassersug, 1984; Wassersug & Murphy, 1987). Adults, which lack a protrusible tongue, use the LJ for biting and prey capture and the CH and hyoglossal plate for supporting the pharynx floor in suction feeding, intraoral transport and lung ventilation (Nishikawa, 2000; Carroño & Nishikawa, 2010).

The AP and TP differ from the rest of the adult PA skeleton in scaling isometrically or positively with body size. As in other aglossan frogs, the AP in *Xenopus* is unusually large and appears to incorporate an anterior hyoglossal process that sometimes forms separately in tongue-feeding frogs (Ridewood, 1897a, 1899; Sedra, 1950; Sedra & Michael, 1957; Chacko, 1965b; de Jongh, 1968). As in most frogs, the TP in *Xenopus* helps support the larynx (Ridewood, 1897a; Sedra & Michael, 1957), which is used for sound production by the adults of both sexes (Tobias et al. 1998, 2014) and is larger in males (Tobias et al. 1991).

The evolutionary significance of the LJ and CH shape trajectories

Morphometric studies of amphibian cranial variation typically focus on entire skulls or skull regions at pre- or post-metamorphic stages to address phylogenetic, functional or developmental questions (Emerson, 1985; Larson, 2002, 2004, 2005, 2008; Jorgensen & Sheil, 2008; Ponssa & Candioti, 2012). This study in contrast focuses on the individual cartilages of a skull region throughout life, and separates their shape trajectories into phases of pre- and post-metamorphic growth and metamorphosis. Quantifying shape trajectories in this manner provides a framework for investigating how cartilage growth and metamorphic remodeling are controlled at the level of individual cell behaviors (Rose, 2009; Slater et al. 2009; Kerney et al. 2012) and affected by mutations and exogenously applied hormones, teratogens and environmental toxins (Huang et al. 1999; Schreiber et al. 2001; Das et al. 2002; Du Preez et al. 2008; Kerney et al. 2012; Vandenberg et al. 2012). Further, comparing multiple cartilages with similar embryonic origins and different functions throughout life reveals how skeletal shape trajectories can be modified by selection on a complex life history (Wassersug & Hoff, 1982; Alberch, 1987, 1989) and at the same time constrained by the cellular and histological properties of cartilage tissue (Rose, 2009).

Xenopus has a relatively unspecialized rod-like LJ that exhibits subtle shape changes in both growth and metamorphosis. In tadpole growth, the LJ increases faster in its anterior–posterior dimension than in its lateral dimension.

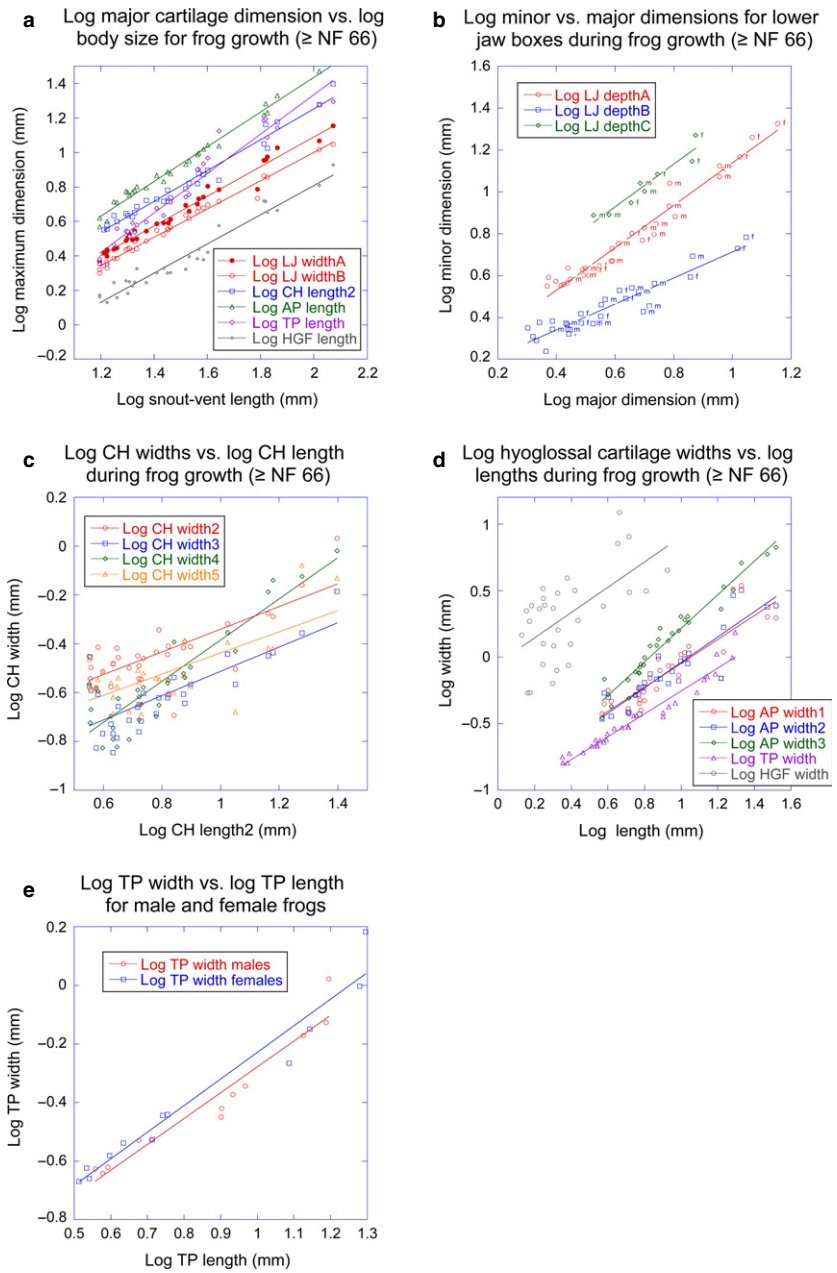

Fig. 6 Size and shape trajectories for PA skeleton for frogs. (a) Log of major dimension of lower jaw (LJ), ceratohyal (CH), alar process (AP), thyroid process (TP) and hyoglossal foramen (HGF) vs. log of body size; (b) log of minor dimension of different LJ rectangles vs. log of their major dimension (f and m indicate sex); (c) log of CH widths vs. log of CH length; (d) log of AP, TP and HGF widths vs. log of their lengths; (e) log of TP width vs. log of TP length for each sex.

Whether this reflects a change in curvature, orientation or both could not be determined by TPSA due to the inability of landmarks to track homologous portions of a cartilage. However, comparing representative shapes at NF 46 and NF 59 (Fig. 4i) suggests that as the MC becomes relatively longer in growth, its anterior portion becomes straighter and more in line with the infrarostral; the alignment of MC and infrarostral is largely complete by mid-tadpole stages (Fig. 2; Sedra, 1950; Trueb & Hanken, 1992). In metamorphosis, the LJ becomes absolutely longer and shorter in its anterior–posterior and lateral dimensions, respectively, and the increase in anterior–posterior dimension is much greater than the increase in actual length (83% vs. 26–35%). This finding highlights the limitations of anatomical studies, which describe the LJ as 'almost doubling in length' but cannot distinguish between changes in actual length and cartilage position (Berry et al. 1998). Comparing representative shapes at NF 58/59 and NF 66 (Figs 2 and 4i) suggests that the LJ shape change involves an increase in curvature medially and an increase in length laterally. In frog growth, the bony LJ grows isometrically, except for becoming more curved laterally soon after sexual maturation. The changes in LJ curvature and length collectively lead to the gape becoming relatively narrower (or deeper) in tadpole growth, absolutely narrower in metamorphosis and relatively wider in frog growth.

The relative lengthening and decreasing curvature of the MC in tadpole growth are interesting because they trans-

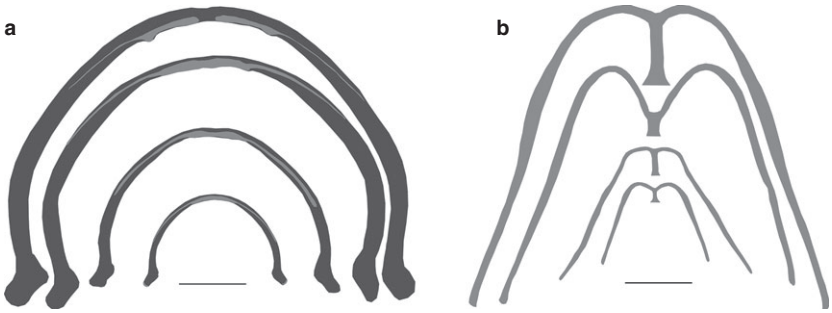

Fig. 7 (a) LJ and (b) CH of representative frogs at sizes spanning frog growth. Ventral views, dark gray is bone, light gray is cartilage, scale bars are 5 mm.

form the post-embryonic LJ of *Xenopus* (NF 46 in Figs 2 and 4i) into a more generalized and less tadpole-like shape (NF 55–59 in the same figures). Most tadpoles have a mobile suprarostral cartilage in the upper jaw and an infrarostral in the LJ that is of similar shape and size to the MC but aligned more laterally, anterolaterally or dorsomedially than the MC to complement the suprarostral (Pusey, 1938; Haas, 1999; Rocek, 2003; Haas et al. 2006, 2014). *Xenopus* tadpoles are distinguished by having their upper jaw skeleton comprised of a broad, immobile suprarostral plate, the edge of which remains straight and does not align with the curving LJ until late tadpole stages (Trueb & Hanken, 1992). Though the NF 46 LJ of *Xenopus* is more typical of tadpoles, this configuration is inconsistent with the lack of a separate suprarostral cartilage and with midwater buccal bumping, which is not expected to require the medial portion of the LJ being differentially aligned or independently mobile. The NF 46 LJ configuration is consistent with the *Xenopus* tadpole evolving from an ancestor with a separate suprarostral cartilage and becoming specialized for midwater suspension feeding by changing the growth of its LJ rather than changing its embryonic patterning.

In contrast to the LJ, the CH in *Xenopus* undergoes negligible shape change during both growth phases, and changes dramatically in both size and shape at metamorphosis. The only similarity between growth and metamorphosis is the shift to a more anteroposterior orientation, which is more pronounced in metamorphosis than in tadpole growth. Unlike PA cartilages in amphibians and fish, which generally resemble gently tapered or straight rods and bars (de Beer, 1937), frog hyoid elements have very diverse shapes (Ridewood, 1897a,b, 1898, 1899; Chacko, 1965a,b; Duellman & Trueb, 1986; Haas, 1999; Rocek, 2003). The relatively heavy tadpole CH in *Xenopus* serves to overcome the flow resistance of the branchial food traps used in midwater suspension feeding (Wassersug & Hoff, 1982; Ryerson & Deban, 2010). The exceptionally narrow adult CH correlates with lack of a tongue and not having to anchor the tongue skeleton during tongue protrusion. Both specializations appear unique to *Xenopus*, and are consistent with complex life histories evolving by the progressive divergence of embryonic and metamorphic patterning (Wassersug & Hoff, 1982; Alberch, 1987). Two other pipid frogs that also lack tongues and suction feed as adults, *Hymenochirus* and *Pipa* (Carroño & Nishikawa, 2010), have apparently diverged in different directions at metamorphosis, one developing a stout, well-ossified adult CH and the other losing its CH altogether (Ridewood, 1897a, 1899).

All rod- and bar-shaped PA cartilages in *Xenopus*, meaning the LJ and CH of tadpoles and the cartilage LJ, CH and TP of frogs, become relatively thinner or narrower during growth. Whether this is also true of plate-shaped cartilages like the AP and those of the pectoral girdle (Trueb & Hanken, 1992) was not addressed in this study. Because it occurs throughout life, relative thinning of cartilages might be a physiological requirement for oxygen supply to keep pace with oxygen demand. As cartilage is avascular, oxygen supply occurs by diffusion across its surface from interstitial fluids, meaning that rates of oxygen supply and demand follow a surface area-to-volume ratio that would decrease if cartilage thickness increased proportionally with size.

The LJ and CH becoming smaller in metamorphosis was not anticipated by hypotheses about how complex life histories evolve (Wassersug & Hoff, 1982; Alberch, 1987, 1989). This is not surprising given that there is no precedent for skeletal tissue becoming smaller in the middle of growth. The decrease in cross-sectional area of the LJ is not accompanied by erosion of surfaces (Sedra & Michael, 1957) but is accompanied by a small increase in length, which supports the hypothesis that rod- and bar-shaped larval cartilages might generally rely upon a spatially integrated mix of cell rearrangement, cell death and cell division to become reshaped into longer, thinner adult cartilages (Rose, 2009; but see Kerney et al. 2012). In contrast, the frog CH emerges from deep within the boundaries of the tadpole CH, which means that the adult element shares no surfaces with the larval element and likely arises from *de novo* morphogenesis within the resorbing larval element (Rose, 2009). Indeed, the sequence of three early NF 66+ stages in Fig. 2 reveals changes in Alcian blue staining that point to rapid changes in cell size and/or matrix secretion in the newly emerged adult CH. Determining whether cartilage size or shape changes of a certain magnitude necessitate a switch from reshaping a larval cartilage to *de novo* morphogenesis of a new adult cartilage and how tadpole cartilage histology relates to the choice of cellular pathway awaits a

comparative histological analysis of amphibian PA skeletal development.

The developmental and evolutionary significance of isometric cartilage growth

The present study is the first to quantify shape change during growth of an amphibian PA skeleton. Notwithstanding the changes in curvature and relative size of the LJ cartilages and relative thinning of most cartilages, growth of the PA skeleton in *Xenopus* is very close to isometric. Isometric growth implies that species-specific aspects (and thus interspecific differences) of cartilage shape arise primarily in embryonic patterning and metamorphic remodeling. This contrasts with parts of the chondrocranium (Larson, 2004, 2005; Jorgensen & Sheil, 2008) and the limb skeleton (Emerson, 1986) in tadpoles of other species, which grow allometrically and exhibit inter- and intraspecific and ecophenotypic variation in shape at the start of metamorphosis.

One possibility for why the PA skeleton of amphibians exhibits geometric similarity in the latter part of larval growth is that it guarantees that metamorphic remodeling proceeds from the same starting shapes regardless of variation in larval growth and developmental rates. Size at the start of metamorphosis in lab-reared *Xenopus laevis* ranges from 0.70 g to more than 1.71 g (Rose, 2014), and the upper limit is likely greater in wild populations (Wager, 1986). Metamorphosis of the PA skeleton in amphibians involves complex, highly coordinated cellular processes that reshape, rearrange and/or rebuild jaw, hyoid and other elements to articulate with each other in new, precisely integrated feeding motions (Alberch & Gale, 1986; Rose & Reiss, 1993; Rose, 2009). The transition is considered to be highly stressful as the animal is poorly adapted to both larval and adult environments, and for a short time unable to feed (Wassersug & Hoff, 1982). A rapid transition to successful adult feeding might thus depend on PA cartilages adhering to tightly constrained pathways of remodeling that start (and thus finish) at fixed shapes.

In contrast, the limb skeleton and parts of the chondrocranium that vary in shape at the start of metamorphosis (references above) exhibit metamorphic changes and post-metamorphic functions that are expected to allow for more variation in larval cartilage shape, some of which could also carry over to post-metamorphic stages. The limbs grow during metamorphosis and their function afterwards is not tied critically to reaching a specific size or shape at the end of metamorphosis (Emerson, 1986). The otic capsule undergoes little change in shape or function at metamorphosis, the muscular process of the tadpole palatoquadrate is lost altogether and the trabecular horn becomes part of the floor of an immobile nasal capsule (de Beer, 1937; Pusey, 1938; Sedra, 1950; Sedra & Michael, 1957; Rocek, 2003).

The regulation of cartilage growth

The present study is also the first to provide evidence for the ability to regulate cartilage shape in normal tadpole growth. The multivariate analyses generally indicate that LJ, CH and BA shapes are more variable and extreme (i.e. different from average) at lower stages than at higher stages. The low spreads of replicate data argue against this being an artifact of measuring small specimens. Also, the LJ, CH and BA shapes at stages with large size ranges are generally more variable and extreme at smaller sizes than at larger sizes. These observations suggest that any shape variation that emerges from embryogeny or arises in young tadpoles is not perpetuated or amplified by either growth (meaning specifically an increase in size) or development (meaning progression through stages). Rather, tadpole growth and development appear to reduce variation, which implies the existence of growth and/or functional feedback mechanisms that detect and correct abnormal shapes. This is supported by a previous report that cartilage shape abnormalities induced by applying teratogens to *Xenopus* embryos tend to be corrected in tadpole growth (Vandenberg et al. 2012).

The existence of mechanisms for regulating cartilage shape during growth has implications for how the PA skeleton evolves in amphibians. Given the self-enclosed nature of cartilage, its role in resisting stress with flexibility and compressibility and its capacity to control tissue shape by coordinating cell behaviors both internally and on its surface (Rose, 2009), the shape-regulating mechanisms that are hypothesized here to direct larval elements to their appropriate starting shapes for metamorphosis might also require them to grow and remodel as cartilage. Such mechanisms would also by definition resist change by local adaptation and ecophenotypic plasticity.

Interestingly, although cranial and articular cartilages in mammals require mechanical stress for normal growth (Herring, 1993; Hall, 2005), there is little evidence that cartilage exhibits adaptive plasticity in shape. Most cranial cartilages in embryonic mammals are constrained by bone, brain and sense organs, and quickly replaced by bone. Food consistency affects the shape and relative size of the condylar cartilage of the mammal mandible (Bouvier & Hylander, 1984; McFadden et al. 1986; Bouvier & Zimny, 1987; Yamada & Kimmel, 1991), but this effect is likely specific to cartilage that is compressed between bones. The PA cartilages of larval amphibians generally do not interface or articulate with bone and, to our knowledge, there are no reports of mechanically induced variation in the shapes of any PA cartilages in larval amphibians or fish including chondrichthyans. Suggestions that growth allometries in ranid tadpole chondrocrania reflect ontogenetic changes in mechanical loading (Larson, 2002) and that intraspecific differences in these allometries arise from food differences (Larson, 2004) are difficult to test. As small suspension feeders, *Xenopus*

tadpoles are not likely to experience much ontogenetic or environmental variation in loading of their PA cartilages. The effect of gravity is offset by buoyancy, no hard material ever contacts any cartilage (Wassersug & Hoff, 1979), and though the LJ, CH and BA experience continual loading when food is available, the greatest stress comes from pumping water from the buccal cavity into the narrow passages of the branchial chamber (Gradwell, 1971; Ryerson & Deban, 2010). Also, whatever changes and differences in mechanical loading occur, amphibian PA cartilages might generally respond to them more at the level of histology than shape.

Setting aside the PA skeleton, it is also worth considering how prevalent isometric growth is in amphibians and in cartilages that receive little or no mechanical loading. Although some post-metamorphic frogs and salamanders appear to grow isometrically in much of their bodies (Sweet, 1980; Emerson, 1978; Kardong, 2012), studies of skull growth and skull differences among species usually indicate otherwise (Birch, 1999; Triepel & Müller, 2014). As far as we know, there are no reports of isometric growth in other relatively unstressed cartilages, though external ear cartilage poses an intriguing model given its variable mobility and function in mammals.

Concluding remarks

Quantifying the size and shape of amphibian cartilages throughout life reveals patterns and directions of ontogenetic change that cannot be gleaned from anatomical studies or morphometric analyses of individual life history periods. Indeed, the LJ of *Xenopus* exhibits subtle changes in curvature in both tadpole and frog growth, and combines changes in curvature, thickness and length at metamorphosis to produce a subtle, but complex shape change that was previously recognized as simply an increase in length. In contrast, the CH of *Xenopus* exhibits little shape change in both growth periods and the adult CH emerges from well within the borders of the larval CH, suggesting that this remodeling is more aptly described as *de novo* morphogenesis. Cartilage thinning, which is relative in growth and absolute in metamorphosis, might reflect an inherent constraint upon cartilage growth that is imposed by using surface diffusion for gas exchange. That PA cartilage growth is otherwise close to isometric and that variation in PA cartilage shape decreases with tadpole growth support the existence of shape-regulating mechanisms that ensure the appropriate starting shapes for metamorphic remodeling. Ongoing research to understand the cellular basis of PA cartilage shape changes might shed insight into these mechanisms. This study also points the way for comparative morphometric and histological analyses to unravel the phylogenetic, functional and developmental influences on post-embryonic cartilage shape in frogs and other vertebrate taxa.

Acknowledgements

The authors thank Melinda Vergara and Whitney Edmonds for help with digitizing landmarks, Kane Nashimoto for statistical consultation, Brian Walton for help using the Shapes package in R, Lennart Olsson for hospitality during the writing, and three anonymous reviewers for helpful comments. This research was supported by NSF grants to CSR (0343838) and BW (DMS-0734284).

Author contributions

CSR and DM prepared, digitized and outlined the NF 46–66 specimens and performed the TPSA and EFA on tadpoles; CSR and VH prepared, digitized and analyzed the specimens used to control for size differences at metamorphosis; CSR, Melinda Vergara and Whitney Edmonds prepared and digitized the NF66+ specimens; and CSR did the remaining analyses, prepared the figures and wrote the paper.

References

Abzhanov A, Tabin CJ (2004) Shh and Fgf8 act synergistically to drive cartilage outgrowth during cranial development. *Dev Biol* **273**, 134–148.

Abzhanov A, Protas M, Grant BR, et al. (2004) Bmp4 and morphological variation of beaks in Darwin's finches. *Science* **305**, 1462–1465.

Abzhanov A, Kuo WP, Hartmann C, et al. (2006) The calmodulin pathway and evolution of elongated beak morphology in Darwin's finches. *Nature* **442**, 563–567.

Alberch P (1987) Evolution of a developmental process: irreversibility and redundancy in amphibian metamorphosis. In: *Development as an Evolutionary Process*. (eds Raff RA, Raff EC), pp. 23–46. New York, NY: Alan R. Liss.

Alberch P (1989) Development and the evolution of amphibian metamorphosis. In: *Trends in Vertebrate Morphology*. (eds Splechtna H, Hilgers H), pp. 163–173. Stuttgart: Gustav Fischer.

Alberch P, Gale EA (1986) Pathways of cytodifferentiation during the metamorphosis of the epibranchial cartilage in the salamander, *Eurycea bislineata*. *Dev Biol* **117**, 233–244.

Alexander RM (1994) *Bones: The Unity of Form and Function*. New York, NY: McMillan.

Alexander RM, Jayes AS, Maloiy GMO, et al. (1979) Allometry of the limb bones of mammals from shrews (*Sorex*) to elephant (*Loxodonta*). *J Zool* **189**, 305–314.

von Baer KE (1828) *Uber Entwicklungsgeschichte der Thiere*. Königsberg: Bornträger.

Ballard WW (1981) Morphogenetic movements and fate maps of vertebrates. *Am Zool* **21**, 391–399.

de Beer GR (1937) *The Development of the Vertebrate Skull*. Oxford: Oxford University Press.

Berry DL, Rose CS, Remo BF, et al. (1998) The expression pattern of thyroid hormone response genes in remodeling tadpole tissues defines distinct growth and resorption gene expression programs. *Dev Biol* **203**, 24–35.

Beverdam A, Merlo GR, Paleari L, et al. (2002) Jaw transformation with gain of symmetry after Dlx5/Dlx6 inactivation: mirror of the past? *Genesis* **34**, 221–227.

Biewener AA (2005) Biomechanical consequences of scaling. *J Exp Biol* **208**, 1665–1676.

Birch JM (1999) Skull allometry in the marine toad, *Bufo marinus*. *J Morphol* **241**, 115–126.

Bouvier M, Hylander WL (1984) The effect of dietary consistency on gross and histologic morphology in the craniofacial region of young rats. *Am J Anat* **170**, 117–126.

Bouvier M, Zimny ML (1987) Effects of mechanical loads on surface morphology of the condylar cartilage of the mandible in rats. *Acta Anat* **129**, 293–300.

Carroll RL (1987) *Vertebrate Palaeontology and Evolution*. New York, NY: W.H. Freeman.

Carroño CA, Nishikawa KC (2010) Aquatic feeding in pipid frogs: the use of suction for prey capture. *J Exp Biol* **213**, 2001–2008.

Chacko T (1965a) The development and metamorphosis of the hyobranchial skeleton in *Rana tigrina*, the Indian bull frog. *Acta Zool - Stockholm* **46**, 1–18.

Chacko T (1965b) The hyolaryngeal apparatus of two anurans. *Acta Zool - Stockholm* **46**, 83–108.

Cooper KL, Oh S, Sung Y, et al. (2013) Multiple phases of chondrocyte enlargement underlie differences in skeletal proportions. *Nature* **495**, 375–378.

Das B, Schreiber AM, Huang H, et al. (2002) Multiple thyroid hormone-induced muscle growth and death programs during metamorphosis in *Xenopus laevis*. *PNAS* **99**, 12 230–12 235.

Depew MJ, Lufkin T, Rubenstein JLR (2002) Specification of jaw subdivisions by Dix genes. *Science* **298**, 381–385.

Dryden IL (2013) *The Shapes Package: Statistical Shape Analysis in R*. Contributed Package. Vienna: R Foundation for Statistical Computing.

Du Preez LH, Kunene N, Everson GJ, et al. (2008) Reproduction, larval growth, and reproductive development in African clawed frogs (*Xenopus laevis*) exposed to atrazine. *Chemosphere* **71**, 546–552.

Duellman WE, Trueb L (1986) *Biology of Amphibians*. New York, NY: McGraw-Hill.

Emerson SB (1978) Allometry and jumping in frogs: helping the twain to meet. *Evolution* **32**, 551–564.

Emerson SB (1985) Skull shape in frogs – correlations with diet. *Herpetologica* **41**, 177–188.

Emerson SB (1986) Heterochrony and frogs: the relationship of a life history trait to morphological form. *Am Nat* **127**, 167–183.

Emerson SB, Bramble DM (1993) Scaling, allometry, and skull design. In: *The Skull., Vol. 3. Functional and Evolutionary Mechanisms* (eds Hanken J, Hall BK), pp. 384–421. Chicago, IL: University of Chicago Press.

Ericsson R, Olsson L (2004) Patterns of spatial and temporal visceral arch muscle development in the Mexican axolotl (*Ambystoma mexicanum*). *J Morphol* **261**, 131–140.

Ericsson R, Cerny R, Falck P, et al. (2004) Role of cranial neural crest cells in visceral arch muscle positioning and morphogenesis in the Mexican axolotl, *Ambystoma mexicanum*. *Dev Dyn* **231**, 237–247.

Ericsson R, Ziermann JM, Piekarski N, et al. (2009) Cell fate and timing in the evolution of neural crest and mesoderm development in the head region of amphibians and lungfishes. *Acta Zool - Stockholm* **90**, 264–272.

Farnum CE, Tinsley M, Hermanson JW (2008a) Forelimb versus hindlimb skeletal development in the big brown bat, *Eptesicus fuscus*: functional divergence is reflected in chondrocytic performance in autopodial growth plates. *Cells Tissues Organs* **187**, 35–47.

Farnum CE, Tinsley M, Hermanson JW (2008b) Postnatal bone elongation of the manus versus pes: analysis of the chondrocytic differentiation cascade in *Mus musculus* and *Eptesicus fuscus*. *Cells Tissues Organs* **187**, 48–58.

Feder ME, Wassersug RJ (1984) Aerial versus aquatic oxygen consumption in larvae of the clawed frog, *Xenopus laevis*. *J Exp Biol* **108**, 231–245.

Galilei G (1638) *Two New Sciences*. Madison, WI: University of Wisconsin Press.

Gendron-Maguire M, Gridley T (1993) Identification of transgenic mice. *Methods Enzymol* **225**, 794–799.

Goodrich ES (1930) *Studies on the Structure and Development of Vertebrates*. London: Macmillan.

Gould SJ (1966) Allometry and size in ontogeny and phylogeny. *Biol Rev* **41**, 587–640.

Gould SJ (1974) The origin and function of 'bizarre' structures: antler size and skull size in the 'Irish Elk', *Megaloceros giganteus*. *Evolution* **28**, 191–220.

Gradwell N (1971) *Xenopus* tadpole: on the water pumping mechanism. *Herpetologica* **27**, 107–123.

Gradwell N (1975) The bearing of filter feeding on the water pumping mechanism of *Xenopus* tadpoles (Anura: Pipidae). *Acta Zool - Stockholm* **56**, 119–128.

Grammatopoulos GA, Bell E, Toole L, et al. (2000) Homeotic transformation of branchial arch identity after Hoxa2 overexpression. *Development* **127**, 5355–5365.

Gregory WK (1933) Fish skulls: a study of the evolution of natural mechanisms. *Trans Am Philos Soc* **23**, 75–481.

Haas A (1999) Larval and metamorphic skeletal development in the fast-developing frog *Pyxicephalus adspersus* (Anura, Ranidae). *Zoomorphology* **119**, 23–35.

Haas A, Hertwig S, Das I (2006) Extreme tadpoles: the morphology of the fossorial megophryid larva, *Leptobrachella mjobergi*. *Zoology* **109**, 26–42.

Haas A, Pohlmeyer J, McLeod DS, et al. (2014) Extreme tadpoles II: the highly derived larval anatomy of *Occidozyga baluensis* (Boulenger, 1896), an obligate carnivorous tadpole. *Zoomorphology* **133**, 321–342.

Haeckel E (1880) *The History of Creation: Or the Development of the Earth and its Inhabitants by the Action of Natural Causes*. New York, NY: Appleton.

Hall BK (1999) *The Neural Crest in Development and Evolution*. New York, NY: Springer.

Hall BK (2005) *Bones and Cartilage, Developmental and Evolutionary Skeletal Biology*. San Diego, CA: Elsevier Academic Press.

Hall JA, Larsen JH Jr (1998) Postembryonic ontogeny of the spadefoot toad, *Scaphiopus intermontanus* (Anura: Pelobatidae): skeletal morphology. *J Morphol* **238**, 179–244.

Herring SW (1993) Epigenetic and functional influences on skull growth. In: *The Skull, Vol. 1. Development*. (eds Hanken J, Hall BK), pp. 153–206. Chicago, IL: University of Chicago Press.

Huang H, Marsh-Armstrong N, Brown DD (1999) Metamorphosis is inhibited in transgenic *Xenopus laevis* tadpoles that overexpress type III deiodinase. *PNAS* **96**, 962–967.

Huxley JA (1932) *Problems of Relative Growth*. London: Methuen.

Irie N, Kuratani S (2011) Comparative transcriptome analysis reveals vertebrate phylotypic period during organogenesis. *Nat Commun* **2**, 248. doi: 10.1038/ncomms1248.

Iwata H, Ukai Y (2002) SHAPE: a computer program package for quantitative evaluation of biological shapes based on elliptic Fourier descriptors. *J Hered* **93**, 384–385.

de Jongh HJ (1968) Functional morphology of the jaw apparatus of larval and metamorphosing *Rana temporaria* L. *Neth J Zool* **18**, 1–103.

Jorgensen ME, Sheil CA (2008) Effects of temperature regime through premetamorphic ontogeny on shape of the chondrocranium in the American Toad, *Anaxyrus americanus*. *Anat Rec* **291**, 818–826.

Kardong KV (2012) *Vertebrates: Comparative Anatomy, Function, Evolution*. New York, NY: McGraw-Hill.

Kerney RR, Brittain AL, Hall BK, et al. (2012) Cartilage on the move: cartilage lineage tracing during tadpole metamorphosis. *Dev Growth Differ* **54**, 739–752.

Kieser JA, Groeneveld HT (1992) Comparative morphology of the mandibulodental complex in wild and domestic canids. *J Anat* **180**, 419–424.

Kuhl FP, Giardina CR (1982) Elliptic Fourier features of a closed contour. *Comput Vision Graph* **18**, 236–258.

Larson PM (2002) Chondrocranial development in larval *Rana sylvatica* (Anura: Ranidae): morphometric analysis of cranial allometry and ontogenetic shape change. *J Morphol* **252**, 131–144.

Larson PM (2004) Chondrocranial morphology and ontogenetic allometry in larval *Bufo americanus* (Anura, Bufonidae). *Zoomorphology* **123**, 95–106.

Larson PM (2005) Ontogeny, phylogeny, and morphology in anuran larvae: morphometric analysis of cranial development and evolution in *Rana* tadpoles (Anura: Ranidae). *J Morphol* **264**, 34–52.

Larson PM (2008) The chondrocrania of North American *Rana* larvae (Anura: Ranidae): a morphological comparison. *Acta Zool - Stockholm* **89**, 279–288.

Mallarino R, Grant PR, Grant BR, et al. (2011) Two developmental modules establish 3D beak-shape variation in Darwin's finches. *PNAS* **108**, 4057–4062.

McFadden LR, McFadden KD, Precious DS (1986) Effect of controlled dietary consistency and cage environment on the rat mandibular growth. *Anat Rec* **215**, 390–396.

McMahon T (1973) Size and shape in biology: elastic criteria impose limits on biological proportions, and consequently on metabolic rates. *Science* **179**, 1201–1204.

McMahon TA (1975) Allometry and biomechanics: limb bones in adult ungulates. *Am Nat* **109**, 547–563.

McNamara KJ (1982) Heterochrony and phylogenetic trends. *Paleobiology* **8**, 130–142.

Miller CT, Yelon D, Stainier DY, et al. (2003) Two endothelin 1 effectors, hand2 and bapx1; pattern ventral pharyngeal cartilage and the jaw joint. *Development* **130**, 1353–1365.

Murray PDF (1936) *Bones. A Study of the Development and Structure of the Vertebrate Skeleton*. Cambridge: Cambridge University Press (reprinted 1985 with an introduction by B. K. Hall).

Nieuwkoop PD, Faber J (1956) *Normal Table of Xenopus laevis* (Daudin). A Systematical and Chronological Survey of the Development from the Fertilized Egg Till the End of Metamorphosis. Amsterdam: North-Holland.

Nishikawa KC (2000) Feeding in frogs. In: *Feeding in Tetrapod Vertebrates: Form, Function, Phylogeny*. (ed. Schwenk K), pp. 117–147. San Diego, CA: Academic Press.

Olsson L, Falck P, Lopez K, et al. (2001) Cranial neural crest cells contribute to connective tissue in cranial muscles in the anuran amphibian, *Bombina orientalis*. *Dev Biol* **237**, 354–367.

Pasqualetti M, Ori M, Nardi I, et al. (2000) Ectopic Hoxa2 induction after neural crest migration results in homeosis of jaw elements in *Xenopus*. *Development* **127**, 5367–5378.

Ponssa ML, Candioti MFV (2012) Patterns of skull development in anurans: size and shape relationship during postmetamorphic cranial ontogeny in five species of the *Leptodactylus fuscus* Group (Anura: Leptodactylidae). *Zoomorphology* **131**, 349–362.

Prange HD, Anderson JF, Rahn H (1979) Scaling of skeletal mass to body mass in birds and mammals. *Am Nat* **113**, 103–122.

Presley R (1993) Preconception of adult structural pattern in the analysis of the developing skull. In: *The Skull*, *Vol. 1. Development*. (eds Hanken J, Hall BK), pp. 347–377. Chicago, IL: University of Chicago Press.

Prothero J (1992) Scaling of bodily proportions in adult terrestrial mammals. *Am J Physiol* **262**, R492–R503.

Prothero DR, Sereno PC (1982) Allometry and paleoecology of medial Miocene dwarf rhinoceroses from the Texas Gulf Coastal Plain. *Paleobiology* **8**, 16–30.

Pusey HK (1938) Structural changes in the anuran mandibular arch during metamorphosis, with reference to *Rana temporaria*. *Q J Microsc Sci* **80**, 479–552.

Pyenson ND, Goldbogen JA, Shadwick RE (2013) Mandible allometry in extant and fossil Balaenopteridae (Cetacea: Mammalia): the largest vertebrate skeletal element and its role in rorqual lunge feeding. *Biol J Linn Soc* **108**, 586–599.

Radinsky LB (1981) Evolution of skull shape in carnivores 1. Representative modern carnivores. *Biol J Linn Soc* **15**, 369–388.

Ridewood WG (1897a) On the structure and development of the hyobranchial skeleton of the parsley-frog (*Pelodytes punctatus*). *Proc Zool Soc Lond* **1897**, 577–594.

Ridewood WG (1897b) On the structure and development of the hyobranchial skeleton and larynx in *Xenopus* and *Pipa*; with remarks on the affinities of the Aglossa. *J Linn Soc Zool* **26**, 53–128.

Ridewood WG (1898) On the development of the hyobranchial skeleton of the midwife-toad (*Alytes obstetricians*). *Proc Zool Soc Lond* **1898**, 4–12.

Ridewood WG (1899) On the hyobranchial skeleton and larynx of the new aglossal toad, *Hymenochirus boettgeri*. *J Linn Soc Zool* **27**, 454–460.

Rijli FM, Mark M, Lakkaraju S, et al. (1993) A homeotic transformation is generated in the rostral branchial region of the head by disruption of Hoxa-2; which acts as a selector gene. *Cell* **75**, 1333–1349.

Rocek Z (2003) Larval development and evolutionary origin of the anuran skull. In: *Amphibian Biology, Vol. 5. Osteology*. (eds Heatwole H, Davies M), pp. 1877–1995. Chipping Norton, NSW, Australia: Surrey Beatty.

Rohlf FJ (2013) Morphometrics at SUNY Stony Brook. http://life.bio.sunysb.edu/morph/.

Rose CS (2003) The developmental morphology of salamander skulls. In: *Amphibian Biology, Vol. 5. Osteology*. (eds Heatwole H, Davies M), pp. 1686–1783. Chipping Norton, NSW, Australia: Surrey Beatty.

Rose CS (2005) Integrating ecology and developmental biology to explain the timing of frog metamorphosis. *TREE* **20**, 129–134.

Rose CS (2009) Generating, growing and transforming skeletal shape: insights from amphibian pharyngeal arch cartilages. *BioEssays* **31**, 287–299.

Rose CS (2014) Caging, but not air deprivation, slows tadpole growth and development in the amphibian *Xenopus laevis*. *J Exp Zool* **321A**, 365–375.

Rose CS, Reiss JO (1993) Metamorphosis and the vertebrate skull: ontogenetic patterns and developmental mechanisms. In: *The Skull*., *Vol. 1. Development* (eds Hanken J, Hall BK), pp. 289–346. Chicago, IL: University of Chicago Press.

Ruhin B, Creuzet S, Vincent C, et al. (2003) Patterning of the hyoid cartilage depends upon signals arising from the ventral foregut endoderm. *Dev Dyn* **228**, 239–246.

Ruibal R, Thomas E (1988) The obligate carnivorous larvae of the frog, *Lepidobatrachus laevis* (Leptodactylidae). *Copeia* **1988**, 591–604.

Russell ES (1916) *Form and Function: A Contribution to the History of Animal Morphology*. London: John Murray.

Ryerson WG, Deban SM (2010) Buccal pumping mechanics of *Xenopus laevis* tadpoles: effects of biotic and abiotic factors. *J Exp Biol* **213**, 2444–2452.

Sadaghiani B, Thiébaud CH (1987) Neural crest development in the *Xenopus laevis* embryo, studied by interspecific transplantation and scanning electron microscopy. *Dev Biol* **124**, 91–110.

Schmidt-Nielsen K (1984) *Scaling. Why is Animal Size So Important*. New York, NY: Cambridge University Press.

Schneider RA, Helms JA (2003) The cellular and molecular origins of beak morphology. *Science* **299**, 565–568.

Schreiber AM, Das B, Huang H, et al. (2001) Diverse developmental programs of *Xenopus laevis* metamorphosis are inhibited by a dominant negative thyroid hormone receptor. *PNAS* **98**, 10 739–10 744.

Schwenk K (2000) *Feeding in Tetrapod Vertebrates: Form, Function, Phylogeny*. San Diego, CA: Academic Press.

Seale DB, Hoff K, Wassersug R (1982) *Xenopus laevis* larvae (Amphibia, Anura) as model suspension feeders. *Hydrobiologia* **87**, 161–169.

Sedra SN (1950) The metamorphosis of the jaws and their muscles in the toad, *Bufo regularis* Reuss, correlated with the changes in the animal's feeding habits. *Proc Zool Soc Lond* **120**, 405–449.

Sedra SN, Michael MI (1957) The development of the skull, visceral arches, larynx and visceral muscles of the South African clawed toad, *Xenopus laevis* (Daudin) during the process of metamorphosis (from stage 55 to stage 66). *Verhandelingen der Koninklijke Nederlandse Akademie van Wetenschappen, Afdeling Natuurkunde. Tweede Reeks* **51**, 1–80.

Sedra SN, Michael MI (1958) The metamorphosis and growth of the hyobranchial apparatus of the Egyptian toad, *Bufo regularis* Reuss. *J Morphol* **103**, 1–30.

Serrat MA (2014) Environmental temperature impact on bone and cartilage growth. *Compr Physiol* **4**, 621–655.

Slater BJ, Liu KJ, Kwan MD, et al. (2009) Cranial osteogenesis and suture morphology in *Xenopus laevis*: a unique model system for studying craniofacial development. *PLoS ONE* **4**, e3914.

Smith L (1920) The hyobranchial apparatus of *Spelerpes bislineata*. *J Morphol* **33**, 527–583.

Strauss RE (1993) The study of allometry after Huxley. In: *Problems of Relative Growth*. (ed. Huxley JA), pp. xlvii–lxxv. Baltimore, MD: Johns Hopkins University Press.

Sweet SS (1980) Allometric inference in morphology. *Am Zool* **20**, 643–652.

Tobias ML, Marin ML, Kelley DB (1991) Development of functional sex differences in the larynx of *Xenopus laevis*. *Dev Biol* **147**, 251–259.

Tobias ML, Viswanathan SS, Kelley DB (1998) Rapping, a female receptive call, initiates male-female duets in the South African clawed frog. *PNAS* **95**, 1870–1875.

Tobias ML, Korsh J, Kelley DB (2014) Evolution of male and female release calls in African clawed frogs. *Behaviour* **151**, 1313–1334.

Triepel S, Müller H (2014) Habitat adaption of salamanders – a morphometric study of *Desmognathus* species (Amphibia: Plethodontidae). Poster. Size and Shape Symposium, Integration of Morphometrics, Mathematical Modelling, Developmental and Evolutionary Biology, Gottingen, Germany.

Trueb L, Hanken J (1992) Skeletal development in *Xenopus laevis* (Anura: Pipidae). *J Morphol* **214**, 1–41.

Vandenberg LN, Adams DS, Levin M (2012) Normalized shape and location of perturbed craniofacial structures in the *Xenopus* tadpole reveal an innate ability to achieve correct morphology. *Dev Dyn* **241**, 863–878.

Wager VA (1986) *Frogs of South Africa: Their Fascinating Life Stories*. Johannesburg, South Africa: Delta Books Pty.

Wake DB (1982) Functional and developmental constraints and opportunities in the evolution of feeding systems in urodeles. In: *Environmental Adaptation and Evolution*. (eds Mossakowski D, Roth G), pp. 51–66. Stuttgart: Gustav Fischer.

Wassersug RJ, Hoff K (1979) A comparative study of the buccal pumping mechanism of tadpoles. *Biol J Linn Soc* **12**, 225–259.

Wassersug RJ, Hoff K (1982) Developmental changes in the orientation of the anuran jaw suspension. In: *Evolutionary Biology*. (eds Hecht MK, Wallace B, Prance GT), pp. 223–246. New York, NY: Plenum.

Wassersug RJ, Murphy AM (1987) Aerial respiration facilitates growth in suspension-feeding anuran larvae (*Xenopus laevis*). *Exp Biol* **46**, 141–147.

van der Westhuizen CM (1961) The development of the chondrocranium of *Heleophryne purcelli* Sclater with special reference to the palatoquadrate and the sound-conducting apparatus. *Acta Zool - Stockholm* **42**, 1–72.

Wiens JJ (1989) Ontogeny of the skeleton of *Spea bombifrons* (Anura: Pelobatidae). *J Morphol* **202**, 29–51.

Wilbur HM, Collins JP (1973) Ecological aspects of amphibian metamorphosis. *Science* **182**, 1305–1314.

Wilder IW (1925) *The Morphology of Amphibian Metamorphosis*. Northampton, MA: Smith College Fiftieth Anniversary Publication.

Wu P, Jiang TX, Suksaweang S, et al. (2004) Molecular shaping of the beak. *Science* **305**, 1465–1466.

Wu P, Jiang TX, Shen JY, et al. (2006) Morphoregulation of avian beaks: comparative mapping of growth zone activities and morphological evolution. *Dev Dyn* **235**, 1400–1412.

Yamada K, Kimmel DB (1991) The effect of dietary consistency on bone mass and turnover in the growing rat mandible. *Arch Oral Biol* **36**, 129–138.

Zelditch MZ, Swiderski DL, Sheets HD, et al. (2004) *Geometric Morphometrics for Biologists: A Primer*. New York, NY: Elsevier Academic Press.

Ziermann JM, Infante C, Hanken J, et al. (2013) Morphology of the cranial skeleton and musculature in the obligate carnivorous tadpole of *Lepidobatrachus laevis* (Anura: Ceratophryidae). *Acta Zool- Stockholm* **94**, 101–112.

Appendix 1: Landmark descriptions

External landmarks for head and body for NF 46–66 (red in Fig. 1a)

E1 Midline tip of snout.
E2 Posterior edge of heart in midline.
E3 Posterior edge of belly in midline.
E4 For NF $\geq$ 56 only, posterior edge of leg in midline.
E5 Where outer edge of head meets anterior curve of pigmented surface of eyeball, ignoring skin fold right next to the eye.
E6 Where outer edge of head meets posterior curve of pigmented surface of eyeball, ignoring skin fold right next to the eye.
E7 Outer edge of head lateral to the most lateral point on the adjacent artery.
E8 For NF < 58, break in curvature or indentation that is anterior of the forelimb and where outermost edge of head meets outermost edge of belly region of body. For NF $\geq$ 58, break in curvature where anterior edge of arm meets outer edge of head, ignoring outer edge of body.
E9 For NF $\geq$ 56 only, break in curvature where posterior edge of belly meets anterior edge of leg, ignoring outer edge of body.

Landmarks for LJ cartilages for NF 46–66 (red in Fig. 1b,c)

LJ1 Most anterior point of IR on midline.
LJ2 Most posterior point of IR on midline.
LJ3 For NF $\leq$ 63 only, most medial point of medial end of MC.
LJ4 For NF $\leq$ 63 only, most anterior point of medial end of MC.
LJ5 Lateral end of MC: most lateral point on anterior edge (anterolateral corner).
LJ6 Lateral end of MC: center of the edge of the bulbous tip.
LJ7 Lateral end of MC: most lateral point on posterior edge (posterolateral corner).
LJ8 For NF $\geq$ 62 only, on posterior edge of MC at the transition between thick medial portion and thin lateral portion.
LJ9 For NF 46–59, halfway along anterior/outer edge of LJ between LJ1 and LJ5. For NF 59–66, break in curvature on the anterior/outer edge of LJ.
LJ10 Counterpoint to LJ9 on posterior/inner edge of MC on a line through LJ9 that is approximately perpendicular to both edges of MC.
LJ11 For NF 59–66 only, on the anterior/outer edge of MC that is at the thinnest part of MC within the first quarter of the distance along the edge from LJ9 to LJ1.
LJ12 For NF 59–66 only, counterpoint to LJ11 on posterior/inner edge of MC on a line through LJ11 that is approximately perpendicular to outer and inner edges of MC.

Landmarks for LJ cartilages and bones for NF $\geq$ 66 (red in Fig. 1d)

LJ1 Most anterior point of LJ on midline.
LJ2 Most posterior point of LJ on midline.
LJ5 Most lateral point of posterior piece of MC.
LJ6 Most posterior point of posterior piece of MC.
LJ7 Posteromedial corner of the bone in the lateral end of LJ.
LJ8 Point on posterior edge of anterior piece of MC at the transition between thick medial portion and thin lateral portion.
LJ13 Point on anterior edge of anterior piece of MC halfway between LJ8 and LJ15.
LJ14 Counterpoint to LJ13 on posterior edge of MC on a line through LJ13 that is approximately perpendicular to both edges of MC.
LJ15 Most posterior point of anterior piece of MC (either tip or center of bulb).
LJ16 Break in curvature of the anterior edge of the lateral end of LJ.
LJ17 Break in curvature of the posterior edge of the lateral end of LJ (center of the 'heel').

Additional landmarks for the bony LJ in large-sized frogs (red in Fig. 1e)

LJ1 Most anterior point of bony LJ on midline (projected from dentary edges if left and right dentaries are not touching in midline).
LJ18 Most lateral point on anterior edge of bony LJ.
LJ19 Counterpoint to LJ18 on posterior edge of bony LJ that is on a line that runs through LJ18 and is approximately perpendicular to both anterior and posterior edges of LJ.
LJ20 Point on anterior edge of bony LJ that is halfway between LJ1 and LJ18.
LJ21 Counterpoint to LJ20 on posterior edge of bony LJ that is on a line that runs through LJ20 and is approximately perpendicular to both edges of LJ.

Landmarks for CH cartilage for NF 46–66 (green in Fig. 1b,c)

CH1 Most medial point on anterior edge of CH (note that left and right CH1s start to converge at NF 62–63).
CH2 Most anterior point on anterior edge of CH.
CH3 Most lateral point of the anterior edge of the CH (anterolateral corner).

CH4 Posterolateral extremity/tip of CH (note that this point becomes the most lateral point on the posterior edge, or new posterolateral corner, of the CH in NF $\geq$ 62).
CH5 Most lateral point on the posterior edge, or posterolateral corner, of the CH (note that this point is lost to resorption of the posterior edge in NF $\geq$ 62).
CH6 Most anterior point on the concave posterior edge of the CH.
CH7 For NF 46–60 only, most medial point on concave posterior edge of CH.
CH8 For NF 46–60 only, most posterior point on straight medial edge of CH.
CH9 For NF 46–61, point on anterior edge of CH on a line that passes through CH6 and is perpendicular to a line through CH5 and CH6. For NF $\geq$ 62, point on anterior edge of CH on a line that passes through CH6 and is perpendicular to the line through CH4 and CH6.
CH10 Posterolateral extremity/tip of CH for NF $\geq$ 63.

Landmarks for CH cartilage for NF $\geq$ 66 (green in Fig. 1d)

CH1 Most medial point on anterior edge of CH (where anterior edges of left and right CHs meet).
CH2 Most anterior point on anterior edge of CH.
CH3 Lateral end of CH: most lateral point on anterior edge
CH4 Lateral end of CH: most lateral point on posterior edge
CH6 Counterpoint to CH2 on concave posterior edge of CH on a line that passes through CH2 and is approximately perpendicular to both edges of CH.
CH7 Medial corner on posterior edge.
CH10 Lateral end of CH: the center between points CH3 and CH4.
CH11 Point on anterior edge of CH about one-third of the length along CH and at its widest part.
CH12 Counterpoint to CH11 on posterior edge of CH on a line through CH11 that is approximately perpendicular to both edges of CH.

Landmarks for BA cartilage for NF 46–60 (yellow in Fig. 1b)

BA1 Most anterior point of branchial basket.
BA2 Medial corner of first gill slit.
BA3 Point where the outline* encounters the lateral end of the first gill slit.
BA4 Indentation in lateral edge of branchial basket.
BA5 Point where the outline* departs from the medial edge of the second slit.
BA6 Point where the outline* encounters the middle of the lateral end of the second slit.
BA7 Point where the outline* encounters the medial end of the third slit.
BA8 Point where the outline* departs from the lateral end of the third slit.
BA9 Most posterior point of branchial basket, ignoring the little extension if present.

*BA2, BA5, BA7, BA8, BA6 and BA3 are landmarked in that order by tracing a smooth outline that encloses the gill slits.

Landmarks for HGF, AP and TP for NF $\geq$ 66 (violet in Fig. 1d)

HGF1 Anterior edge of HGF in midline.
HGF2 Posterior edge of HGF in midline.
AP1 Most posterior point on concave anteromedial edge of AP.
AP2 Most posterior point on posterior tip of AP.
AP3 Counterpoint to AP4 on lateral edge of AP on a line through AP4 that is perpendicular to the central axis of the AP.
AP4 Lateral edge of HGF approximately halfway along its length.
AP5 Lateral edge of AP approximately halfway along its length and where lateral and medial edges appear parallel to each other.
AP6 Counterpoint to AP5 on medial edge of AP on a line through AP5 that is perpendicular to the central axis of the AP.
AP7 Lateral edge of alar process approximately three-quarters along its length and where alar process reaches maximal width.
AP8 Counterpoint to AP7 on medial edge of AP on a line through AP7 that is perpendicular to the central axis of the AP.
TP1 Where lateral edge of TP meets medial edge of AP (larger specimens) or cartilage ring around HGF (smaller specimens).
TP2 Most posterior point on posterior tip of TP.
TP3 Lateral edge of TP approximately halfway along its length.
TP4 Counterpoint to TP3 on medial edge of TP on a line through TP3 that is perpendicular to the central axis of the TP.

Appendix 2: Criteria for calculating body size and dimensions from photographs

Body size dimensions (Fig. 1a):

SBL: E1 to E3.
Head length: E1 to E2.
Head width1: E5L to E5R.
Head width2: E7L to E7R.

Cartilage dimensions (Fig. 1b–d):

LJ widthA, depthA: LJ6L to LJ6R, midpoint of widthA line to LJ1.

LJ widthB, depthB: LJ15L to LJ15R, midpoint of widthB line to LJ1.
LJ widthC, depthC: LJ18L to LJ18R, midpoint of widthC line to LJ1.
LJ outer length: LJ1 to LJ5 following cartilage edges as closely as possible.
LJ inner length: LJ2 to LJ7 following cartilage edges as closely as possible.
LJ width1 (unpaired, at median end of IR): LJ1 to LJ2.
LJ width2 (at median end of MC): LJ4 to LJ3.
LJ width3 (at lateral end of LJ): LJ5 to LJ7.
LJ width4 (at middle of LJ): LJ9 to LJ10.
LJ width5 (at thinnest part of LJ): LJ11 to LJ12 in NF 59–66, LJ13 to LJ14 in NF $\geq$ 66.
LJ width6 (at concavity near joint): LJ16 to LJ17.
LJ width7 (at widest part of gape): LJ18 to LJ19.
LJ width8: LJ20 to LJ21.
CH length1 for NF 46–66: CH1 to CH4.
CH length2 for $\geq$ NF 66: CH2 to CH10.
CH width1 for NF 46–66: CH6 to CH9.
CH width2 for NF $\geq$ 66: CH11 to CH12.
CH width3 (at anterior inflection point): CH2 to CH6.
CH width4 (at posterior tip): CH3 to CH4.
AP length: AP1 to AP2.
AP width1: AP3 to AP4.
AP width2: AP5 to AP6.
AP width3: AP7 to AP8.
TP length: TP1 to TP2.
TP width: TP3 to TP4.
HGF length: HGF1 to HGF2.
HGF width: AP4L to AP4R.